An abundant merozoite surface protein of *Plasmodium falciparum* modulates susceptibility to inhibitory antibodies

Isabelle G. Henshall[1], Jill Chmielewski[1], Dimuthu Angage[2], Ornella Romeo[1], Keng Heng - Lai[1, 3], Kaitlin R. Turland[1, 3], Nicki Badii[2], Michael Foley[2, 4], Robin F. Anders[2], James Beeson[5, 6,7] and Danny W Wilson[1, 3, 5, *].

[1]Research Centre for Infectious Diseases, School of Biological Sciences, The University of Adelaide, Australia 5005

[2]Department of Biochemistry and Chemistry, La Trobe Institute for Molecular Sciences, La Trobe University, Victoria, Australia 3086

[3]Institute for Photonics and Advanced Sensing (IPAS), University of Adelaide, 5005, SA, Australia

[4]AdAlta, 15/2 Park Drive, Bundoora, Victoria, Australia 3083

[5]Burnet Institute, 85 Commercial Road, Melbourne 3004, Victoria, Australia

[6]Department of Infectious Diseases, University of Melbourne, Victoria, Australia

[7] School of Translational Medicine and Department of Microbiology, Monash University, Victoria, Australia

*Corresponding Author: danny.wilson@adelaide.edu.au

Abstract

Malaria merozoite surface proteins (MSPs), are thought to have important roles in red blood cell (RBC) invasion and their exposure on the parasite surface makes them attractive vaccine candidates. However, their role in invasion has not been directly demonstrated and their biological functions are unknown. One of the most abundant proteins is *Pf*MSP2, which is likely an ancestral protein that has been maintained in the *Plasmodium falciparum* lineage and is a focus of vaccine development, whose function remains unknown. Using CRISPR-Cas9 gene-editing, we removed *Pf*MSP2 from two different *P. falciparum* lines with no impact on parasite replication or phenotype *in vitro*, demonstrating that it is not essential for RBC

invasion. However, loss of *Pf*MSP2 led to increased inhibitory potency of antibodies targeting other merozoite proteins involved in invasion, particularly *Pf*AMA1. In a solid-phase model, increasing concentrations of *Pf*MSP2 protein reduced binding of different antibodies against *Pf*AMA1 in a dose dependent manner. These data suggest that *Pf*MSP2 can modulate the susceptibility of merozoites to protective inhibitory antibodies. The results of this study change our understanding of the potential functions of *Pf*MSP2 and establishes a new concept in malaria where a surface protein can reduce the protective efficacy of antibodies targeting a different antigen. These findings have important implications for understanding malaria immunity and informing vaccine development.

Introduction

Plasmodium falciparum malaria remains a global health challenge with over half a million deaths annually (World Health Organization, 2024). Worryingly, increasing parasite resistance to frontline antimalarials and mosquito insecticide resistance are decreasing the effectiveness of key control measures (World Health Organization, 2024). Development of the RTS,S and R21 vaccines targeting the *P. falciparum* circumsporozoite protein is a step forward for malaria vaccine development, however further improvements in vaccine efficacy and longevity are needed to protect those most at risk – children under 5 years – and enable malaria elimination (Beeson et al., 2019; Datoo et al., 2024; RTSS Clinical Trials Partnership, 2015). Understanding the function of vaccine targets remains important for prioritisation and optimisation of candidates in the development pipeline. Merozoites, the parasite stage that invades host red blood cells (RBCs), have long been targeted for vaccine development since successful blocking of merozoite invasion would prevent the repeated cycles of blood-stage parasite multiplication and associated disease. While much work has been done to understand the processes and steps required for merozoite invasion, only a few merozoite proteins have successfully had functions defined. To date, most vaccines based on merozoite antigens have demonstrated limited efficacy (Beeson et al., 2016) at least in part due to the extensive polymorphisms exhibited by many of these antigens.

The surface of the merozoite is covered in a fibril coat which is comprised of multiple proteins, broadly known as merozoite surface proteins (MSPs). These proteins have been proposed to mediate weak initial merozoite RBC contact (Bannister et al., 1986; Beeson et al., 2016; Cowman et al., 2017; Weiss et al., 2015) and in *P. falciparum* are dominated by GPI-anchored

proteins, the most abundant being *Pf*MSP1 and 2 (Gilson et al., 2006). *Pf*MSP1 has been suggested to have a role in merozoite attachment to the RBC (Li et al., 2004), but recent evidence instead suggests that it has a role in merozoite rupture from schizonts and cellular interaction studies using optical tweezers do not support a substantial role for this protein in RBC binding (Das et al., 2015; Kals et al., 2024), although it may have another function in invasion. These recent insights into *Pf*MSP1 function, the best studied MSP, highlight what little is known of MSPs and their roles in parasite survival.

P. falciparum merozoite surface protein 2 (*Pf*MSP2), a protein proposed to be essential for parasite growth (Sanders et al., 2006), has been of long-term interest as a vaccine candidate. *Pf*MSP2 is a ~28 kDa intrinsically disordered protein that has conserved N- and C- termini, along with a central variable region that defines two main allelic groups, 3D7-like and FC27-like (Adda et al., 2012). While *Pf*MSP2 was theorised to have a mechanical role in the early steps of invasion (Anders et al., 2010), there is minimal supporting evidence for this, in part due to the lack of tools to study *Pf*MSP2 function. Studies with recombinant proteins suggest that it is likely *Pf*MSP2 interacts with lipids and forms complexes with itself on the merozoite surface (Adda et al., 2009; Lu et al., 2019; Zhang et al., 2012). *Pf*MSP2 peptides have also been reported to bind the RBC and inhibit *P. falciparum* growth, which would support *Pf*MSP2 mediating merozoite-RBC interactions (Ocampo et al., 2003). Unlike the majority of the merozoite surface coat proteins, *Pf*MSP2 is not present in other malaria parasites that infect humans and has been postulated to have evolved specifically in the *Laverania* subgenus of *Plasmodium*, which includes *P. falciparum* (Black et al., 2002).

*Pf*MSP2 has been trialled in a vaccine (Combination B) combined with fragments of *Pf*MSP1 and *Pf*RESA. A Phase 1/2b trial of this vaccine showed efficacy in reducing the parasite burden in children, which was specific to the *Pf*MSP2 3D7-like allele used in the vaccine formulation (Genton et al., 2003). Vaccine-induced antibodies from clinical trials or experiments in animals have little or no inhibitory activity in standard growth inhibition assays (Boyle et al., 2015; McCarthy et al., 2011), but did show functional activity through the recruitment of complement, promoting opsonic phagocytosis and antibody-dependent cellular inhibition (Boyle et al., 2015; Feng et al., 2018; McCarthy et al., 2011). Naturally acquired antibodies are also known to target *Pf*MSP2 and have been linked to protection (Fowkes et al., 2010; Osier et al., 2010; Stanisic et al., 2009; Zerebinski et al., 2024). Studies have highlighted that it is the Fc-mediated functional activities of these naturally acquired *Pf*MSP2 antibodies, as opposed to direct blocking of *Pf*MSP2 protein function, that correlates best with protection (Boyle et

al., 2015, 2014; Osier et al., 2014; Reiling et al., 2019). While *Pf*MSP2 is a key target of naturally acquired malaria immunity, little is known about the function of *Pf*MSP2, hindering its advancement as a potential vaccine candidate.

Here we take a reverse genetics approach to assess the function of *Pf*MSP2, quantifying the impacts of *Pf*MSP2 deletion on parasite invasion and phenotype. Given our findings that deletion of MSP2 did not impact invasion *in vitro*, we tested the alternative hypothesis that merozoite surface proteins may function to modulate susceptibility of merozoites to inhibitory antibodies.

Results

Avian malaria MSP2-like proteins are structurally similar to *Laverania* MSP2s and show that MSP2 did not arise exclusively in this clade.

Genome annotations of *pfmsp2* show it lies between the merozoite surface protein *pfmsp5* (PF3D7_0206900) and *pfmsp*4 (PF3D7_0207000), and the conserved purine biosynthesis enzyme *adenylosuccinate lyase* (ADSL, PF3D7_0206700) (Figure 1A) (PlasmoDB; (Aurrecoechea et al., 2009)), with this arrangement previously thought to be restricted to the *Laverania* clade which includes parasites that infect great apes and *P. falciparum* (Black et al., 2002; Ferreira et al., 2015). As described by Escalante et al. (2022), we found the genomes of the two annotated avian *Plasmodium* spp. available on PlasmoDB, *P. relictum* and *P. gallinaceum*, to also have a putative gene between ADSL and MSP5 with structural similarities to *Laverania* MSP2s. The reduced length of the *P. relictum* (PRELSG_0415300) and *P. gallinaceum* (PGAL8A_00017700) MSP2-like proteins compared to those of *Laverania* parasites is accounted for by the absence of any extended central domains of the two avian malaria parasites (Supplementary Figure 1).

Given the estimated that ~10 million years of evolution separate the avian malaria parasites *P. relictum* and *P. gallinaceum* from the *Laverania* (Böhme et al., 2018), we explored whether similarities in amino acid sequence and predicted conformation would support a shared lineage and functional properties of these putative MSP2s. Although *Pf*MSP2 is generally considered

126 a disordered protein with limited conservation, the hydrophobic N- and C-terminal sequences
127 that correspond to secretion signals (SP) and GPI-attachment signals, as well as short regions
128 downstream and upstream of these signal sequences respectively, show significant
129 conservation across *P. falciparum* MSP2s. Here we compared the sequence similarity of these
130 conserved regions between the *Laverania* and avian MSPs and found consistently high levels
131 of conservation for the putative SP (>89% similarity) (Supplementary Figure 1), the 24 amino
132 acid N-terminal conserved region (78% similarity) that has a propensity for alpha-helical
133 structure and fibril formation (Yang et al., 2010) (Supplementary Figure 2), the 50 amino acid
134 residue C-terminal conserved region (62% similarity) (Supplementary Figure 3) and the C-
135 terminal GPI signal sequence (>79%), including the presence of short side chain amino acids
136 that mark predicted GPI cleavage sites (Eisenhaber et al., 1999)(Smythe et al., 1991)(Gilson et
137 al., 2006) (Supplementary Figure 1). *Laverania* MSP2s contain two C-terminal cysteine
138 residues that form an intramolecular disulphide bond (Zhang et al., 2008). This arrangement
139 of 2 C-terminal cysteines is found in *P. gallinaceum* MSP2, but not *P. relictum* which has only
140 one (Supplementary Figure 3). Overall, these N and C-terminal conserved regions show broad
141 conservation in properties across the *Laverania* and avian malarias which could contribute to
142 a conserved sub-cellular localisation.

143 Characteristic of *P. falciparum* MSP2s is the dimorphic central variable repeat region that are
144 grouped as 3D7 or FC27-like amino acid sequence structures. A defining feature of the 3D7-
145 like MSP2 family are 4 or 8-mer tandem repeats consisting of small amino acids (for 3D7: Gly,
146 Gly, Ser, Ala) (MacRaild et al., 2015; Smythe et al., 1991). The FC27-like MSP2 family also
147 has repeats of 12 or 32 amino acids in length, but these do not resemble those of the 3D7-like
148 family. We found that the non-*P. falciparum Laverania* and avian malaria MSP2 sequences
149 also contained >75% small amino acids (some of: Gly, Ser, Ala, Thr) repeats, but the exact
150 number (4 to 8 repeats), length (3 to 7 amino acids) and the level of conservation between
151 repeats differed between and within species (Supplementary Figure 4). Broadly speaking, these
152 *Laverania* and avian malaria MSP2 repeats had a 3D7-like repeat structure, with no example
153 of a FC27-like repeat structure identified even with an additional nine *Laverania* MSP2s from
154 the NCBI experimental database compared (data not shown). This comparison highlights the
155 surprising finding that a region of known dimorphic variability in *P. falciparum* MSP2 is likely
156 to retain functional constraints that favour small amino acid rich repeats immediately
157 downstream of the N-terminal conserved region.

158 Extensive studies on recombinant proteins of the *P. falciparum* 3D7 and FC27 variants of
159 *Pf*MSP2 have shown this merozoite surface protein to be intrinsically disordered. Given the
160 evidence for conservation of the primary structure of MSP2s from distantly related malaria
161 parasites, we used AlphaFold2 predictions (Jumper et al., 2021) to examine whether there were
162 likely to be also conformational similarities between *Laverania* MSP2s and those of *P. relictum*
163 and *P. gallinaceum*. The MSP2s in the database of AlphaFold2-predicted structures retain their
164 N- and C-terminal signal sequences, but as these are both absent from mature MSP2 on the
165 merozoite surface they were deleted from the MSP2 sequences used for the AlphaFold2
166 predictions reported here. The predicted structures of the two avian parasite MSP2s, and other
167 *Laverania* MSP2s, are very similar to that of *Pf*3D7 MSP2, with most of the polypetide chains
168 lacking predicted secondary structure and, from the colour coding, have a predicted local
169 distance test (pLDDT) consistent with that of an intrinsically disordered protein over the
170 majority of the proteins length (Figure 1B). In contrast to the rest of the polypeptide, some α-
171 helical structure was predicted in the conserved 20-residue N-terminal region of all the
172 *Laverania* and avian MSP2s. NMR studies with recombinant *Pf*3D7 and *Pf*FC27 MSP2
173 showed this conserved N-terminal sequence to have a propensity for forming an α-helix that
174 was stabilized in the presence of lipid mimetics (MacRaild et al., 2012). The low pLDDT
175 values are consistent with this region in the other *Laverania* and *P. gallinaceum* MSP2 having
176 some propensity for α-helix formation, whereas higher pLDDT values suggest the possible
177 presence of a more stable α-helix in this region of *P. relictum* MSP2.

178 Having established that MSP2 is present across different *Plasmodium* lineages sharing similar
179 predicted amino acid compositions and structural features, the phylogenetic relationship
180 between annotated *Laverania* and putative avian malaria parasite MSP2s was examined. A
181 phylogenetic tree was generated based on alignments of representative sequences from each
182 species. MSP2 sequences from species belonging to the *Laverania* subgenus all grouped
183 together with two smaller clusters, corresponding to the known *Laverania* clade A and clade
184 B species (Figure 1C). As expected, *P. relictum* and *P. gallinaceum* MSP2 also group together.
185 The phylogenetic tree generated based on MSP2 sequences mirrors the proposed evolution of
186 *Plasmodium* spp. (Figure 1C). As postulated by Escalante et al. (2022) , these data suggest that
187 MSP2 was likely present in the ancestral *Plasmodium* parasite prior to the split of the
188 mammalian infecting *Plasmodium* spp. from those that infect birds and lizards. Given the
189 shared amino acid sequence and predicted conformational similarities, including the high levels
190 of intrinsically disordered sequence outside of the N- and C-terminal regions, the *P. relictum*

191 and *P. gallinaceum* MSP2-like proteins appear likely to contain enough properties to
192 potentially be functionally equivalent to *Laverania* MSP2s. This conservation of MSP2-like
193 proteins across different species suggests it has an important function.

194

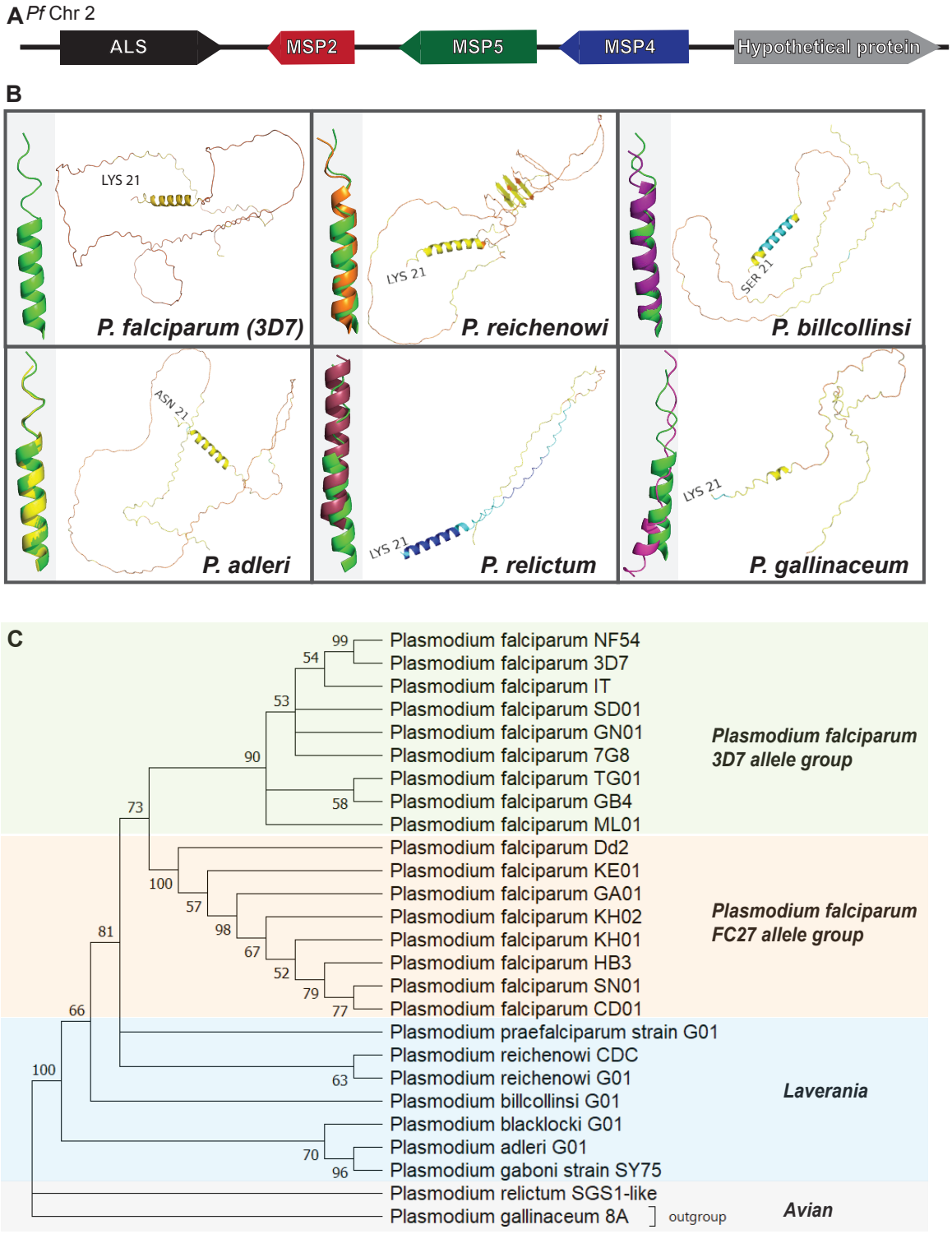

195

196 **Figure 1.** Presence and structure of MSP2 across different *Plasmodium* species. **(A)** Schematic
197 of the gene arrangement surrounding *msp2* on *P. falciparum* chromosome 2. **(B)** AlphaFold2
198 structural predictions of example *Laverania* (*P. falciparum* (3D7), *P. reichenowi*, *P.*
199 *billcollinsi*, *P. adleri*) and the two avian (*P. relictum*, *P. gallinaceum*) malaria species. The N-
200 terminal signal peptide and C-terminal GPI anchor sequences were removed before the proteins
201 structure was predicted. The most N-terminal amino acid is indicated. Colours represent the
202 predicted local distance difference test (pLDDT) scores, with dark blue representing very high
203 confidence (>90%), light blue high confidence (90 to >70), yellow low confidence (70 to 50)
204 and orange very low confidence (<50). An enlarged modelled structure of the N-terminal
205 helical region is provided for *P. falciparum* 3D7 MSP2 on the left of the panel (grey shading),
206 and also for the other examples of *Laverania* and avian MSPs (various colours) superimposed
207 on the structure of *P. falciparum* 3D7 MSP2 (green). **(C)** Maximum likelihood tree showing
208 relationship of MSP2 protein sequences found in different *P. falciparum* isolates and other
209 *Plasmodium* species. Grouping of sequences from *P. falciparum* isolates into two main allele
210 types can be seen as well as the separation of the *Laverania* and avian malaria species into their
211 expected groups. Tree robustness tested by bootstrap.

212

213 **Loss of *Pf*MSP2 does not noticeably impact growth or invasion of different *P. falciparum***
214 **lines *in vitro*.**

215 Given previous unsuccessful attempts to disrupt *pfmsp2* (Sanders et al., 2006), and its high
216 abundance on the merozoite surface (Gilson et al., 2006), *Pf*MSP2 has been traditionally
217 viewed as an essential *P. falciparum* protein with an essential function in merozoite invasion.
218 We employed CRISPR-Cas9 gene editing to determine whether the reported inability to knock-
219 out *pfmsp2 in vitro* was a result of this protein being essential for parasite survival or because
220 of the lower efficiency of the previously used gene-editing system (Sanders et al., 2006).
221 Unexpectedly, we confirmed successful disruption of *pfmsp2* by replacing the coding sequence
222 between 132 bp and 819 bp of the gene with a hDHFR drug selection cassette in the 3D7 *P.*
223 *falciparum* laboratory-adapted line (Figure 2A and B), resulting in *Pf*3D7 ΔMSP2 parasites.
224 We confirmed that *Pf*MSP2 was no longer expressed in *Pf*3D7 ΔMSP2 parasites by western
225 blot, which detected a MSP2 band around 50 kDa in *Pf*3D7 WT parasite material but not in
226 *Pf*3D7 ΔMSP2 parasites (Figure 2C). Similarly, immunofluorescence microscopy using anti-
227 *Pf*MSP2 rabbit polyclonal antibodies showed the expected surface localisation of MSP2 on

228 *Pf*3D7 WT merozoites but not on *Pf*3D7 ΔMSP2 parasites (Figure 2D). We next assessed
229 whether knock-out of *Pf*MSP2 impacted on parasite growth over one or two cycles of
230 development *in vitro* and found that deletion of *Pf*3D7 MSP2 did not cause any significant
231 change in growth (Figure 2E and F).

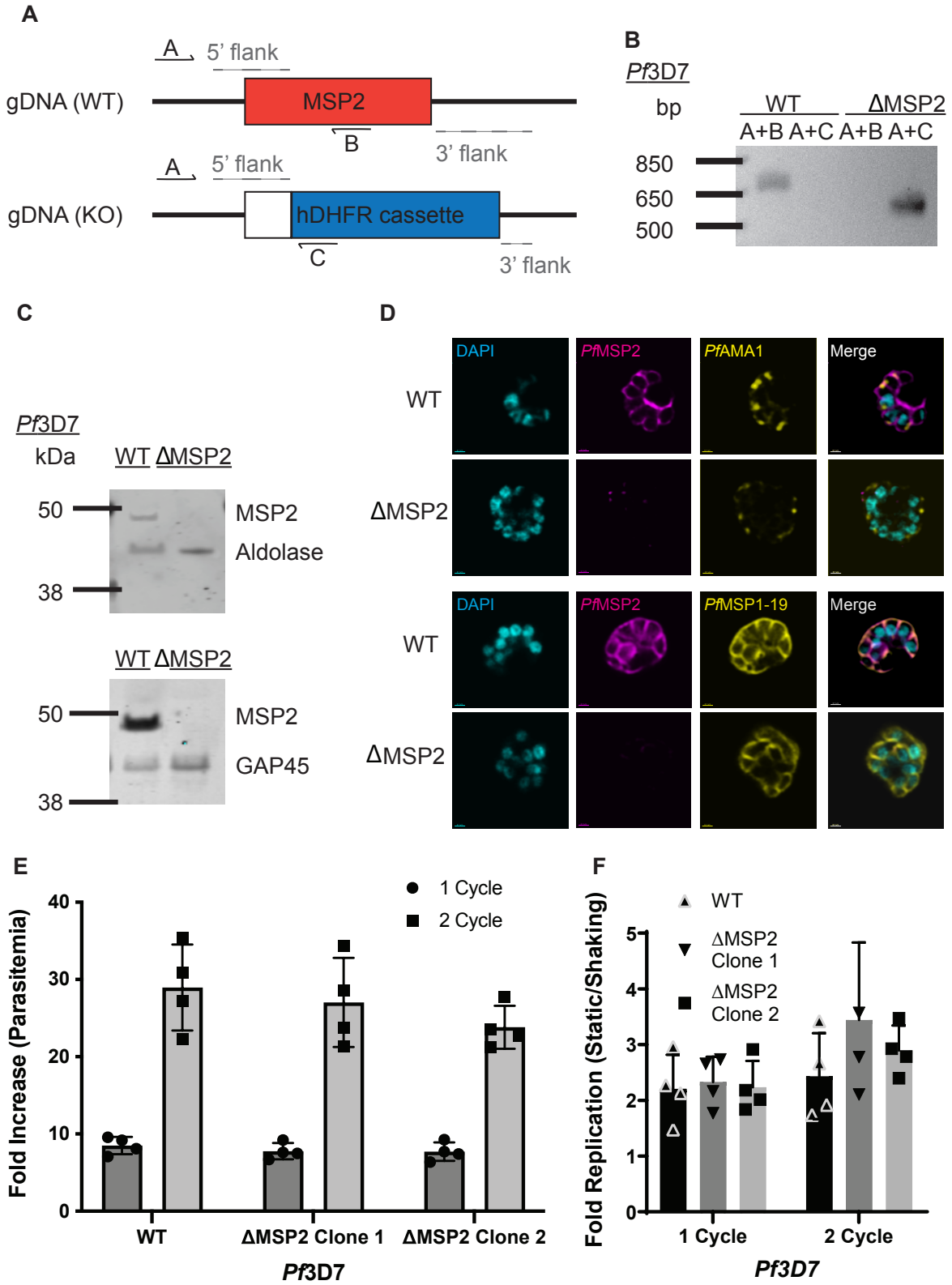

232

233 **Figure 2.** *Pf*MSP2 is not essential for growth *in vitro* of *Pf*3D7 blood stage parasites. **(A-B)**
234 Schematic and agarose gel showing integration of knockout construct (band A+C) in the
235 *msp2* gene locus and absence of the *msp2* sequence from the *Pf*3D7 ΔMSP2 line (band A+B).
236 **(C)** Western Blot of late schizont protein extracts confirms no *Pf*MSP2 is expressed in the
237 *Pf*3D7 ΔMSP2 line. *Pf*MSP2 detected by anti-*Pf*MSP2 2F2 3D7 mAb with *Pf*Aldolase (upper
238 blot) or *Pf*GAP45 (lower blot) serving as loading and stage of expression controls
239 respectively. Representative image shown. **(D)** Distribution of key merozoite surface proteins
240 in the presence or absence of *Pf*MSP2 was visualised by immunofluorescence. *Pf*MSP2
241 (magenta), the nucleus stained by DAPI (cyan) and *Pf*AMA1 (yellow, top two rows) or
242 *Pf*MSP1-19 (yellow, bottom two rows), and the coloured merge of the preceding panels.
243 Scale bar = 0.7 µm. Representative images shown from a minimum of 10 schizonts imaged
244 per condition. **(E-F)** Growth of *Pf*3D7 WT compared to *Pf*3D7 ΔMSP2 *P. falciparum*
245 parasites, measured as fold increase in parasitaemia, over one (48 hrs) or two (96 hrs) cycles
246 in either standard (still- (E)) or shaking (F) conditions, with no measurable difference
247 between parasite growth rates seen between standard or shaking conditions. Parasitaemia was
248 determined by flow cytometry at the start and end to calculate fold increase. Graph displays
249 mean ± S.D. of three independent experiments performed with technical triplicates.
250 Significance determined by unpaired t-test with $p < 0.05$ deemed significant.

251

252

253 As *Pf*MSP2 has been considered, to this point, as essential for *P. falciparum* growth *in vitro*
254 (Sanders et al., 2006), we investigated whether *Pf*MSP2 could also be removed from *Pf*Dd2,
255 an isolate of *P. falciparum* that differs from 3D7 in geographical origin, RBC receptor usage
256 and allelic type of *pfmsp2*. Using CRISPR-Cas9 we successfully knocked-out *msp2* in *Pf*Dd2
257 (Figure 3 A and B) and confirmed the absence of the protein in *Pf*Dd2 ΔMSP2 parasites using
258 western blot (Figure 3C). As we found for *Pf*3D7, deletion of *Pf*Dd2 *msp2* did not result in a
259 significant impact on parasite growth over one or two cycles of parasite replication (Figure
260 3D).

261 Given the abundance of *Pf*MSP2 on the merozoite surface, we postulated that loss of this
262 protein may impact on the timing of merozoite invasion of the RBC, which is not reflected in
263 reduced growth in *in vitro* cultures. Previous studies using live-cell microscopy have reported
264 that merozoites first contact the RBC and form weak initial interactions. The merozoite then

265 reorientates to bring apical organelles into position to release their contents onto the RBC,
266 which then leads to formation of the tight junction, merozoite invasion through the tight-
267 junction, formation of the parasitophorous vacuole and resealing of the RBC membrane post-
268 entry (Weiss et al., 2015). Given its surface localization, *Pf*MSP2 has been speculated to act in
269 the early phase of merozoite attachment. To assess whether knock-out of *pfmsp2* impacted on
270 the progression of invasion, we used live-cell microscopy of *Pf*Dd2 ΔMSP2 parasites and
271 compared the timing and key steps of invasion to *Pf*Dd2 WT parasites *in vitro*. This analysis
272 showed that, although there was a trend for *Pf*Dd2 ΔMSP2 knock-out parasites to have a higher
273 mean time to attach to the RBC, as well as for the length and strength of RBC deformation,
274 these trends did not reach significance. For those merozoites that did invade the RBC, on
275 average it took less time for *Pf*Dd2 ΔMSP2 knock-out parasites to invade then *Pf*Dd2 WT, but
276 this again did not reach significance (Figure 3 E-H). Together these data show *Pf*MSP2 is not
277 essential for blood-stage replication *in vitro* in two *P. falciparum* laboratory isolates from
278 different geographical regions and knock-out of *Pf*MSP2 does not seem to significantly impact
279 parasite growth or merozoite invasion *in vitro*. However, its conservation across diverse
280 *Plasmodium* spp. suggests it does play an important function or is advantageous for parasite
281 survival.

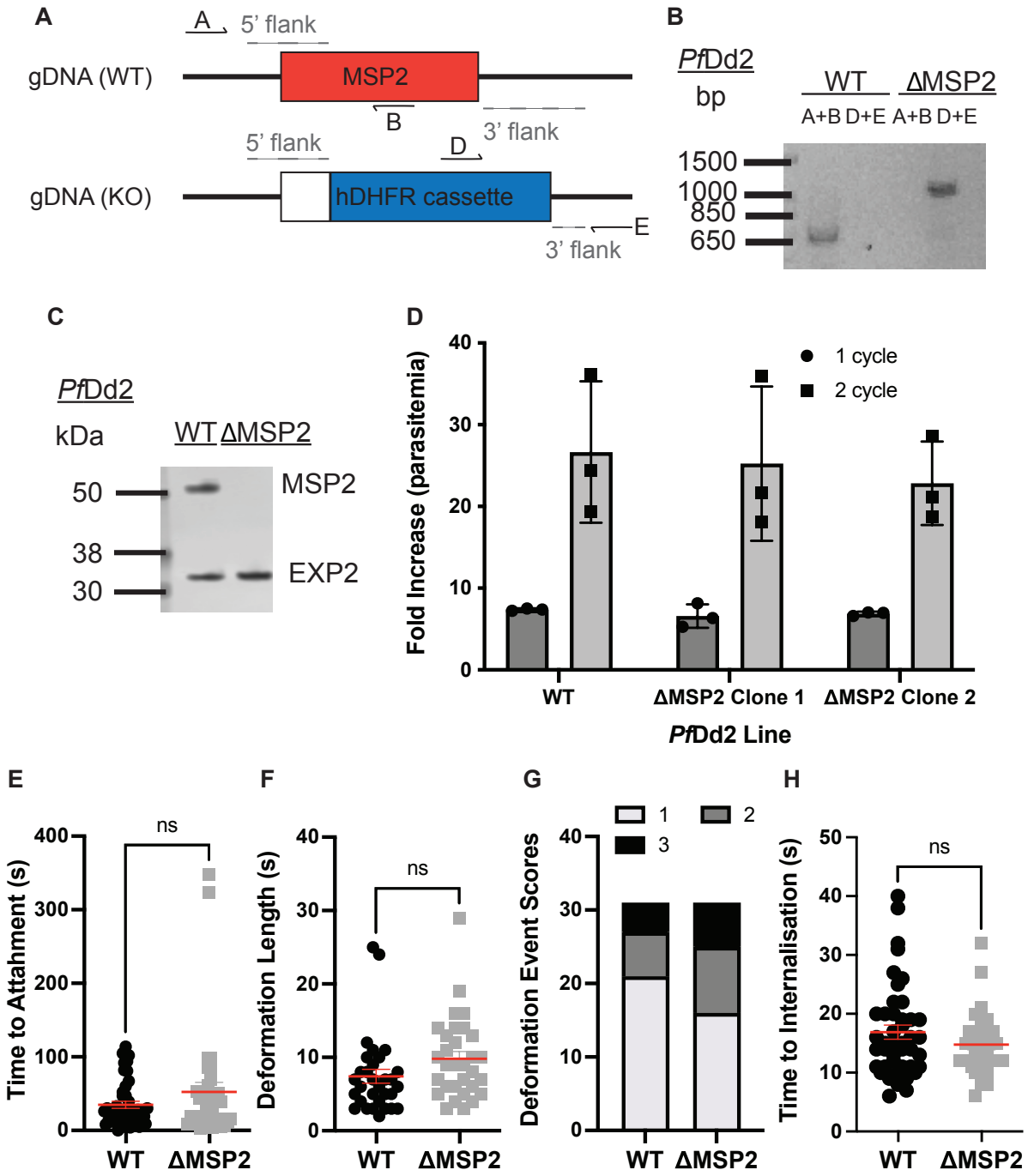

Figure 3. *Pf*Dd2 does not require MSP2 for asexual growth *in vitro*. **(A-B)** Successful integration of KO construct (schematic in A) into the *msp2* gene locus of *Pf*Dd2 ΔMSP2 was confirmed by PCR of genomic DNA (primers A+B amplify WT locus, primers D+E amplify integrated KO construct). **(C)** Loss of *Pf*MSP2 expression was demonstrated by western blot of schizont protein extract with *Pf*MSP2 detected by anti-*Pf*MSP2 FC27 and anti-*Pf*EXP2 as

289 loading control. Representative image shown. **(D)** Growth of *Pf*Dd2 WT *P. falciparum*
290 parasites and *Pf*Dd2 ΔMSP2 over one (48 hrs) or two (96 hrs) cycles. Parasitaemia was
291 determined by flow cytometry at the start and end to calculate fold increase. Graph displays
292 mean ± S.D. of three independent experiments performed with technical triplicates. **(E-H)**
293 Key parameters of merozoite invasion were measured for both *Pf*Dd2 WT and *Pf*Dd2
294 ΔMSP2 parasites that had successfully invaded a RBC using live cell imaging of merozoite
295 invasion. Time to merozoite attachment to RBCs **(E)**, length **(F)** and strength **(G)** of RBC
296 deformation, and time to complete merozoite invasion **(H)** were measured by live
297 microscopy. Deformation scores are as defined by Weiss et al (2015), with 1 = weak
298 deformation of the RBC membrane at the point of contact, 2 = strong deformation leading to
299 the RBC membrane extending up the sides of the merozoite and changes in RBC membrane
300 curvature beyond the point of contact and 3 = extreme deformation indicated by the
301 merozoite being deeply embedded in the RBC membrane and strong deformation of the RBC
302 well beyond the point of contact. A minimum of 30 invading merozoites for each line were
303 captured and assessed. Significance determined by unpaired t-test with $p < 0.05$ deemed
304 significant.

305

306 **Impact of MSP2 gene deletion on gene expression and invasion pathway usage.**

307 Because of the close proximity of the *pfmsp*2, 4 and 5 genes on chromosome 2, similarities in
308 their structure (e.g. GPI-anchor intrinsically disordered protein) and shared merozoite surface
309 localization, we used qPCR to assess whether knock-out of *Pf*3D7 MSP2 impacted the
310 expression levels of *Pf*3D7 MSP4 or MSP5. We found no change in MSP4 and MSP5
311 expression levels between *Pf*3D7 ΔMSP2 parasites and *Pf*3D7 WT parasites (Figure 4A). As
312 expected, *Pf*MSP2 was not detected in the *Pf*3D7 ΔMSP2 parasites.

313 Secreted *P. falciparum* antigens belonging to the erythrocyte binding antigen (EBA) and
314 reticulocyte binding homologue (Rh) families are known to facilitate host-cell invasion through
315 specific receptors on the RBC surface. Reliance on specific EBA or Rh proteins, or their
316 cognate host-cell receptor, define different invasion pathways that can be crudely described by
317 the sensitivity of merozoite invasion to cleavage of RBC surface proteins with trypsin,
318 chymotrypsin and neuraminidase (Baum et al., 2005; Duraisingh et al., 2003; Orlandi et al.,
319 1992).When we assessed whether *Pf*MSP2 knock-out impacted merozoite invasion pathway

usage, we found that *Pf*3D7 ΔMSP2 parasites grew equally as well as *Pf*3D7 WT parasites in all enzyme-treated RBCs (Figure 4B).

To investigate whether *Pf*MSP2 knock-out caused any changes in gene-expression of proteins that may have a role in merozoite invasion and possibly compensate for loss of *Pf*MSP2, we undertook RNA sequencing and differential gene expression analysis of *Pf*3D7 ΔMSP2 and *Pf*3D7 WT parasites. As expected, the *Pf*MSP2 transcript, which was targeted for removal by our CRISPR-Cas9 strategy, was not detected in the *Pf*3D7 ΔMSP2 parasites between 132 bp and 819 bp (Supplementary Figure 5). After removal of genes belonging to variant surface antigen families from the data, eight transcripts were found to have a log2fold expression increase above 1; none of these proteins are annotated as a merozoite surface or secreted protein linked to merozoite invasion (Figure 4C, Table 1). Five of these eight upregulated proteins are of unknown function and expressed at schizont stages, and only one (*Pf*3D7_0909100) has a transmembrane domain that could possibly anchor it to a membrane surface as the GPI anchor does for *Pf*MSP2 (Table 1). Three proteins were found to have a log2fold expression of <-1, indicating a significant reduction in expression with *Pf*MSP2 knock-out, with *Pf*MSP2 being one of these and the other two predicted to be exported proteins (Figure 4C, Table 1). While these data do not exclude any of the *Plasmodium* proteins with unknown function that are upregulated in *Pf*3D7 ΔMSP2 parasites as having a role that compensates for the loss of *Pf*MSP2, only one is predicted to have a transmembrane domain that would bind it to a membrane and no protein identified as up or down-regulated with *Pf*MSP2 knock-out has previously been linked to merozoite invasion. Therefore, *Pf*MSP2 knock-out does appear to have led to changes in gene expression, but does not appear to have a significant impact on the regulation of known merozoite surface or secreted protein gene-expression that would suggest loss of *Pf*MSP2 is compensated for by another protein.

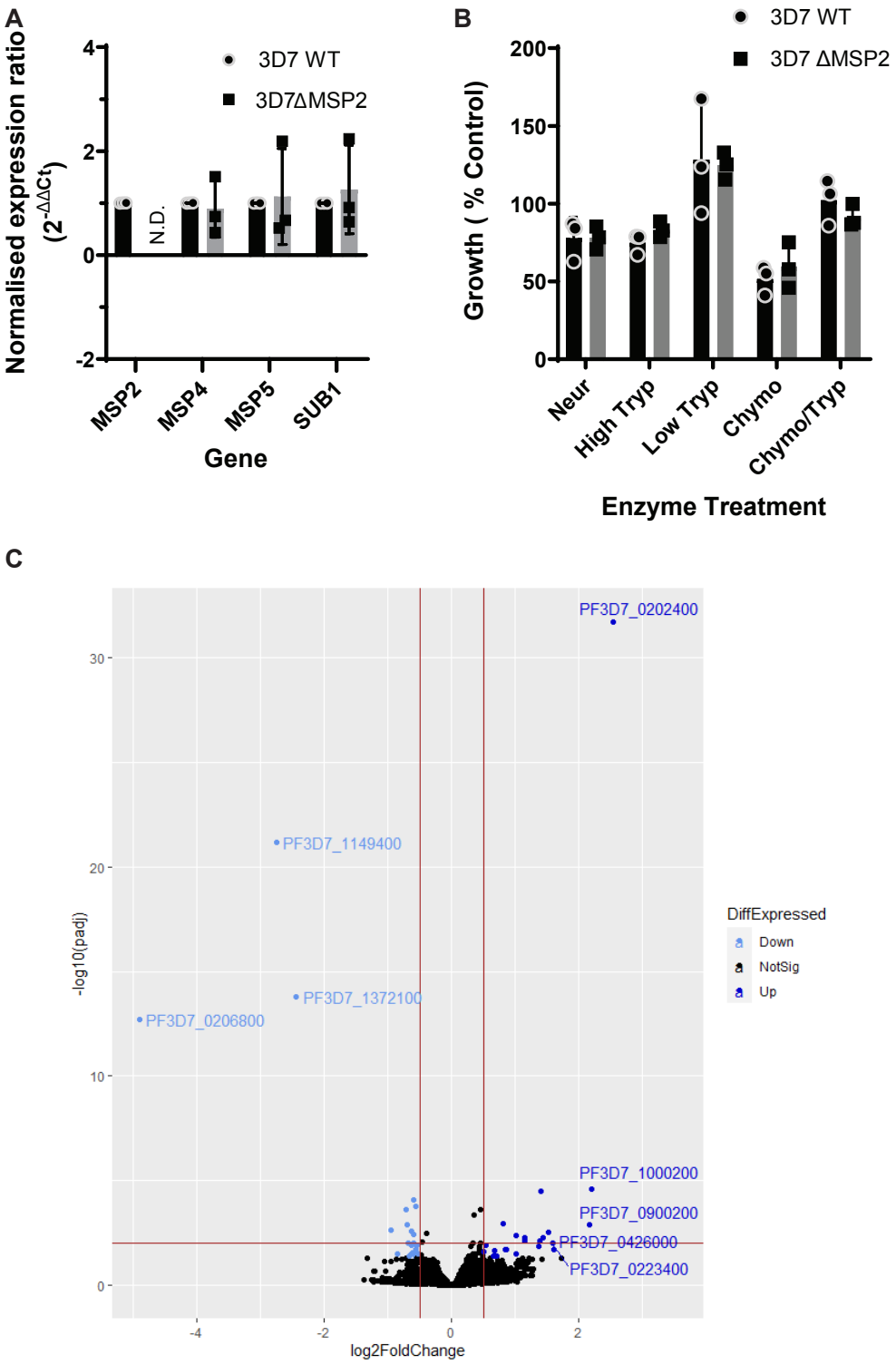

Figure 4. The impact of the loss of *Pf*MSP2 on expression of known merozoite invasion genes and invasion pathway utilization. **(A)** Impact of *Pf*MSP2 KO on schizont transcript abundance was assessed by qPCR for genes located in proximity to *Pfmsp*2 on chromosome 2. Changes in expression between *Pf*3D7 WT and *Pf*3D7 ΔMSP2 parasites was determined by qPCR

350 relative to *pfaldolase* expression with *pfsub1* serving as a schizont stage control. Graph displays
351 mean ± S.D. of three independent RNA harvests. **(B)** Selective enzymatic cleavage of key RBC
352 receptors showed no difference in invasion preference between *Pf*3D7MSP2 WT and *Pf*3D7
353 ΔMSP2 parasites. Parasitaemia was determined by flow cytometry and compared to growth in
354 non-treated control RBCs. Graph displays mean ± S.D. of three independent experiments. **(C)**
355 Log2(fold change) for differentially expressed genes, including multigene families, between
356 the transcriptome of *Pf*3D7 WT and *Pf*3D7 ΔMSP2 schizonts. Plot represents the results for
357 one of four independent schizont RNA harvests for *Pf*3D7 WT and *Pf*3D7 ΔMSP2 parasites
358 and red lines differentiate genes with a log2 (fold change) > 0.5 and < -0.5 with adjusted p-
359 value < 0.01. Genes shaded blue represent those genes that were found to have an average log2
360 (fold change) > 0.5 (dark blue) or < -0.5 (light blue) across the four replicate samples compared.
361 Significance determined as below p< 0.05 after correction for multiple testing.

362

363 **Impact of *Pf*MSP2 disruption on antibodies and inhibitors targeting secreted surface**
364 **exposed antigens**

365 Merozoites are key targets of antibodies during malaria infection with antibodies either able to
366 directly block protein function and thus merozoite invasion, or recruit effectors such as
367 complement leading to the destruction of the merozoite (Beeson et al., 2016). Given the
368 prominence of *Pf*MSP2 on the merozoite surface we asked the question; how does the loss of
369 *Pf*MSP2 affect antibody efficacy against merozoites?

370 *Pf*EBAs and *Pf*Rhs moderate early steps in invasion with a degree of redundancy between these
371 proteins. Several EBAs and Rhs can be targeted with invasion inhibitory antibodies and are
372 targets of acquired human antibodies (Persson et al., 2013, 2008; Richards et al., 2013). We
373 found no significant difference in the ability of purified rabbit immunoglobulin raised against
374 single (*Pf*Rh2b) or combinations of *Pf*EBAs and *Pf*Rhs (*Pf*EBA175/*Pf*Rh2b,
375 *Pf*EBA175/*Pf*Rh4, *Pf*EBA175/*Pf*Rh2b/*Pf*Rh4) to inhibit growth of *Pf*3D7 WT or *Pf*3D7
376 ΔMSP2 parasites (Figure 5A). Similarly, knock-out of MSP2 in *Pf*Dd2 did not significantly
377 change the parasites sensitivity to rabbit antibodies raised against isogeneic W2mef EBA175
378 (Figure 5B). Broadly speaking, these results mirror what was seen with selective cleavage of
379 the RBC ligands of *Pf*EBAs and *Pf*Rhs using enzyme treatment of RBCs (Figure 4B), with no
380 evidence that loss of *Pf*MSP2 changed either the importance of these secreted merozoite
381 antigens during invasion or their sensitivity to antibodies targeting different antigens.

382 The interaction of *Pf*Rh5 with RBC surface receptor basigin is a critical, non-redundant
383 interaction for *P. falciparum* merozoite invasion and a known target of direct invasion-
384 inhibitory antibodies (Alanine et al., 2019; Crosnier et al., 2011; Douglas et al., 2011). *Pf*Rh5
385 was the initial member of the PCRCR complex to be described, with subsequent studies
386 demonstrating that antibodies against other members of this complex could also block
387 merozoite invasion of the RBC (Scally et al., 2022). Given the importance of these secreted
388 antigens to current vaccine development efforts, we next investigated whether loss of *Pf*MSP2
389 impacted on the parasite's sensitivity to antibodies targeting these antigens. There was no
390 difference in sensitivity between *Pf*3D7 WT and *Pf*3D7 ΔMSP2 parasites when treated with
391 invasion-inhibitory rabbit antibodies targeting *Pf*Rh5 (Figure 5C) or nanobodies targeting
392 PCRCR complex component *Pf*PTRAMP (H8) (Figure 5D). Nanobodies targeting the PCRCR
393 complex component CSS (D2) showed a slight, but non-significant increase in invasion-
394 inhibitory activity in the absence of *Pf*MSP2 (1.4-fold increase; IC_{50} value for *Pf*3D7 WT is 57
395 μg/mL; IC_{50} value for *Pf*3D7 ΔMSP2 is 42 μg/mL; p=0.3; Figure 5E). However, the *Pf*3D7
396 ΔMSP2 specific increase in invasion-inhibitory activity was amplified with the addition of the
397 human Fc domain to the anti-CSS nanobody (D2-Fc) to be 3-fold greater for *Pf*3D7 ΔMSP2
398 parasites (IC_{50} *Pf*3D7 WT 138 μg/mL; IC_{50} *Pf*3D7 ΔMSP2 46 μg/mL; p=0.0001; Figure 5F).

399 The glycosaminoglycan heparin is a specific inhibitor of invasion and has been observed to
400 bind to the 42 kDa C-terminal region of *Pf*MSP1 the most abundant GPI-anchored protein on
401 the merozoite surface, marking this as a possible mechanism for its invasion inhibitory activity
402 (Boyle et al., 2010a). However, the highly charged state of heparin means that it could block
403 invasion through binding additional proteins. When tested against *Pf*3D7 WT and *Pf*3D7
404 ΔMSP2 parasites, we observed a small increase in inhibitory potency of heparin for parasites
405 lacking *Pf*MSP2 (1.4-fold; IC_{50} *Pf*3D7 WT 0.65 IU/mL; IC_{50} *Pf*3D7 ΔMSP2 0.47 IU/mL;
406 p=0.0003; Figure 5G). We next tested rabbit antibodies raised against the C-terminal 19 kDa
407 fragment of *Pf*MSP1. We found a small but non-significant trend towards increased inhibition
408 of growth in parasites that lacked *Pf*MSP2 across repeat experiments (Figure 5H). These data
409 suggest that loss of *Pf*MSP2 can impact on the invasion-inhibitory potency of some antibodies
410 that target secreted or surface antigens.

411

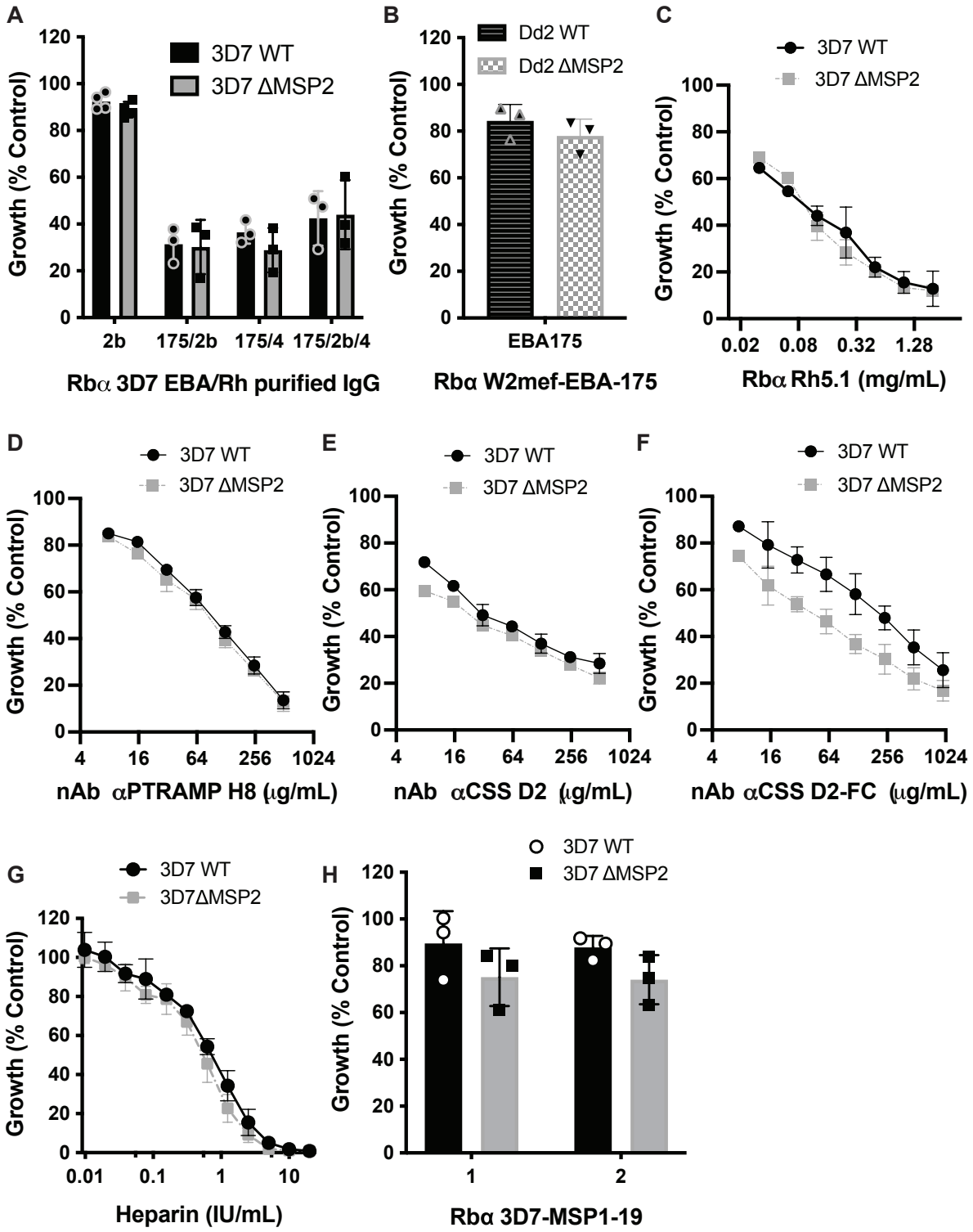

Figure 5. Impact of *Pf*MSP2 removal on efficacy of antibodies targeting other merozoite surface-exposed antigens. Changes in antibody efficacy in the absence of *Pf*MSP2 was assessed by measuring changes in antibody invasion inhibition and subsequent growth compared to growth in the absence of antibody for both *P. falciparum* WT and ΔMSP2

417 parasites over 2 cycles. **(A)** Rabbit (Rb) IgG raised against merozoite antigens of the *Pf*3D7
418 EBA/Rh family. **(B)** Rabbit sera raised against *Pf*Dd2 EBA175. **(C)** Rabbit IgG raised against
419 *Pf*3D7 Rh5. **(D)** Nanobody (nAb) to *Pf*3D7 PTRAMP. **(E-F)** Nanobody and Fc-tagged
420 nanobody to *Pf*3D7 CSS. **(G)** The invasion inhibitory glycosaminoglycan heparin. **(H)** Rabbit
421 sera raised against *Pf*3D7 MSP1-19 (different vaccinated rabbit sera identified by numbers).
422 Graph displays mean ± S.D. of three different experiments. Significance was determined by
423 unpaired t-test when only a single concentration point was tested and for IC_{50} comparisons an
424 extra Sum-of-Squares F Test (best-fit $LogIC_{50}$) was performed with $p< 0.05$ deemed
425 significant.

426

427

428 **Loss of *Pf*MSP2 consistently potentiates AMA1 invasion inhibitory antibodies**

429 Subsequent to *Pf*Rh5 -basigin binding in the steps of merozoite invasion is the formation of the
430 tight-junction between *Pf*AMA1, secreted from the micronemes onto the merozoite surface,
431 and the rhoptry neck protein *Pf*RON2, which is inserted into the RBC membrane (Lamarque
432 et al., 2011; Srinivasan et al., 2011). In lines where *Pf*MSP2 was disrupted, we found a
433 consistent potentiation of antibodies that had anti-*Pf*AMA1 invasion-inhibitory activity.
434 Invasion-inhibitory polyclonal rabbit serum antibodies and purified immunoglobulin raised
435 against *Pf*AMA1 of *Pf*3D7 and *Pf*W2mef (isogenic to *Pf*Dd2), which express different alleles
436 of both *Pf*MSP2 and *Pf*AMA1, were found to be more inhibitory with *Pf*MSP2 knock-out
437 (Figure 6A and B). The polyclonal antibody with the greatest potentiation of inhibitory activity
438 was an IgG preparation purified from a rabbit antiserum raised against *Pf*W2mef AMA1. This
439 had a 3-fold increased potency against *Pf*Dd2 ΔMSP2 compared to *Pf*Dd2 WT (IC_{50} *Pf*Dd2
440 WT 0.015 mg/mL; IC_{50} *Pf*Dd2 ΔMSP2 0.005 mg/mL; $p<0.0001$) over two cycles of growth
441 (Figure 6B, C).

442 The mouse 1F9 (binds to the RON2 binding pocket and polymorphic loop 1d (Coley et al.,
443 2007)) and rat 4G2 (binds to a conserved epitope in the ectodomain (Kocken et al., 1998))
444 monoclonal antibodies have been shown to target different regions of *Pf*AMA1 and exhibit
445 selective inhibition against *Pf*3D7 AMA1. Here we found potentiation of invasion inhibitory
446 activity with *Pf*3D7 MSP2 knock-out for both 1F9 (2.1-fold; IC_{50} *Pf*3D7 WT 0.27 mg/mL; IC_{50}
447 *Pf*3D7 ΔMSP2 0.13 mg/mL; $p<0.0001$; Figure 6D) and 4G2 (3.2-fold; IC_{50} *Pf*3D7 WT 1.15
448 mg/mL; IC_{50} *Pf*3D7 ΔMSP2 0.36 mg/mL; $p<0.0001$; Figure 6E).

449 We also tested the invasion inhibitory effect of i-bodies, which are smaller single-domain
450 antibody-like molecules inspired from the shark variable new antigen receptor (V_{NAR})
451 (Griffiths et al., 2016a, 2018). When we tested the i-body WD34 (Angage et al., 2024) which
452 binds a highly conserved epitope that includes the *Pf*RON2-binding pocket on *Pf*AMA1, we
453 observed a small potentiation of *Pf*AMA1 specific activity with knock-out of *Pf*MSP2 in *Pf*3D7
454 (1.3-fold; IC_{50} *Pf*3D7 WT 0.012 mg/mL; IC_{50} *Pf*3D7 ΔMSP2 0.009 mg/mL; p=0.08 Figure 6F).
455 Given WD34 was also found to be inhibitory to growth of W2mef parasites (Angage et al.,
456 2024) we also tested its activity against our *Pf*Dd2 ΔMSP2 parasites and found potentiation of
457 invasion inhibitory activity with loss of MSP2 in *Pf*Dd2 parasites (2-fold; IC_{50} *Pf*Dd2 WT
458 0.016 mg/mL; IC_{50} *Pf*Dd2 ΔMSP2 0.008 mg/mL; p=0.004 Figure 6G). As was observed for
459 the anti-CSS nanobody, addition of a human Fc domain to WD34 amplified the inhibitory
460 phenotype, with WD34 Fc having a 2.3-fold greater inhibitory activity against *Pf*3D7 ΔMSP2
461 than against *Pf*3D7 WT (IC_{50} *Pf*3D7 WT 0.1 mg/mL; IC_{50} *Pf*3D7 ΔMSP2 0.04 mg/mL;
462 p=0.0004; Figure 6H). A second i-body, WD33 (Angage et al., 2024), which binds AMA1
463 between domain II and domain III, had very limited invasion inhibitory activity against *Pf*3D7
464 parasites and did not show improved potency with knock-out of *Pf*3D7 MSP2 (0.9-fold; IC_{50}
465 *Pf*3D7 WT 1.02 mg/mL; IC_{50} *Pf*3D7 ΔMSP2 1.1 mg/mL; p=0.8; Figure 6I). Although the
466 limited inhibitory activity for WD33 tagged with the Fc receptor prevented us determining an
467 IC_{50} at the concentrations feasible to test, there was no increased inhibition of *Pf*3D7 ΔMSP2
468 parasites compared to the low level seen with *Pf*3D7 WT parasites (data not shown). These
469 data suggest that the potentiation of *Pf*AMA1 targeted antibody inhibition with MSP2 knock-
470 out is *Pf*AMA1 epitope dependent.

471 To account for the differences in i-body sizes, we compared the WD34 and WD34 Fc i-bodies
472 on a molar basis and found that they had similar activities against *Pf*3D7 MSP2 WT parasites
473 (IC_{50} 0.94 μM and 1 μM respectively) indicating that the Fc-tag itself did not modify epitope
474 binding properties. Rather, it is the absence of *Pf*MSP2 that results in increased inhibition of
475 AMA1 function by WD34, and this is further potentiated by antibody size.

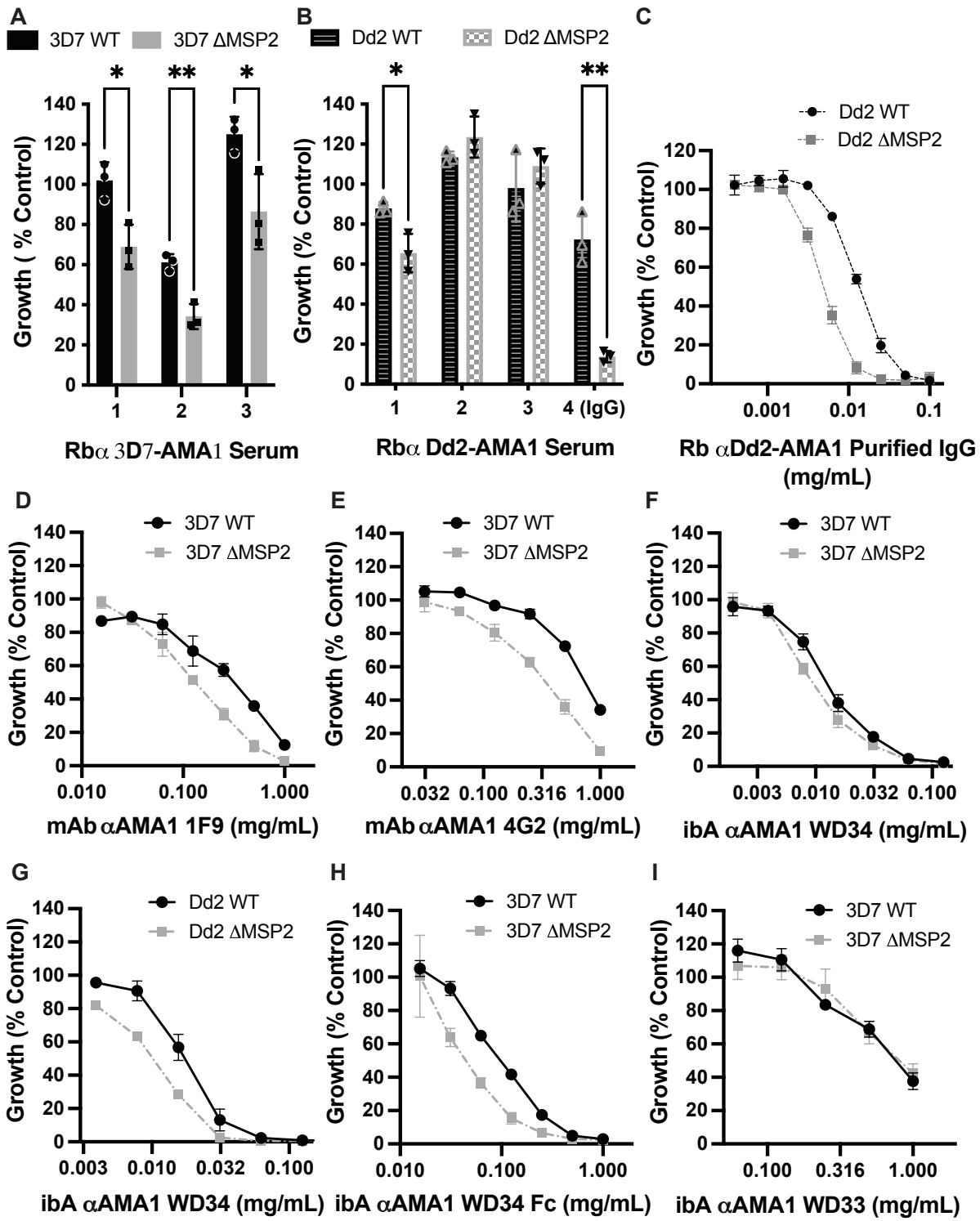

Figure 6. Absence of *Pf*MSP2 from the merozoite surface impacts invasion inhibition by *Pf*AMA1 antibodies. *Pf*3D7 **(A, D-F, H, I)** and *Pf*Dd2 **(B, C, G)** express different *Pf*MSP2 alleles and different *Pf*AMA1 alleles, yet both showed altered anti-AMA1 antibody growth inhibition in the absence of *Pf*MSP2. The effect was seen with serum (**A-B**; different vaccinated rabbit (Rb) sera identified by numbers), purified rabbit and mouse monoclonal

481 (mAb) antibodies **(C-E)** and i-bodies (ibA) **(F-J)**. Final parasitaemia was determined by flow
482 cytometry and compared to control. Graph displays mean ± S.D. of three or four independent
483 experiments. Significance was determined by unpaired t-test when only a single concentration
484 point was tested and for IC_{50} comparisons an extra Sum-of-Squares F Test (best-fit $LogIC_{50}$)
485 was performed with $p < 0.05$ deemed significant.

486

487 In light of these results, we hypothesised that removal of *Pf*MSP2 may improve antibody access
488 to other antigens that are targets of inhibitory antibodies. To assess whether this was the case,
489 we first tested whether increased *Pf*AMA1 polyclonal antibody binding to the surface of
490 merozoites could be observed for *Pf*3D7 ΔMSP2 compared to *Pf*3D7 MSP2 WT parasites using
491 a fluorescently tagged WD34 i-body (WD34-mCherry) for quantitative immunofluorescence
492 assays of late stage schizonts labelled with a single incubation and wash step. We observed
493 WD34-mCherry to have a significantly higher mean fluorescence intensity for *Pf*3D7 ΔMSP2
494 compared to *Pf*3D7 WT (Figure 7A), supporting that the *Pf*AMA1 i-bodies may have better
495 access in the absence of *Pf*MSP2. As a control, we tested labelling using a fluorescently tagged
496 WD33 i-body which binds to AMA1 (Angage et al., 2024), but we found did not have improved
497 inhibitory activity in the absence of MSP2 (Figure 6I). Mirroring the results of the growth
498 assay, there was no difference observed for WD33-eGFP binding fluorescence for *Pf*3D7
499 ΔMSP2 compared to *Pf*3D7 WT parasites (Figure 7B).

500 We next explored whether the addition of recombinant *Pf*MSP2 could impact on the inhibitory
501 antibody binding on-rate against substrate-bound *Pf*AMA1 recombinant protein using Surface
502 Plasmon Resonance (SPR). For the anti-*Pf*AMA1 targeting mAb 4G2, there was a non-
503 significant trend toward a lower on-rate in the presence of recombinant *Pf*MSP2 (Figure 7C).
504 For the i-body WD34-Fc, there was minimal difference in detectable binding to *Pf*AMA1 in
505 the presence or absence of *Pf*MSP2 (Figure 7C). Using a similar principle of testing antibody
506 binding to substrate-bound *Pf*AMA1 protein in the presence, or absence of increasing
507 concentrations of *Pf*MSP2, we assessed changes in levels of anti-*Pf*AMA1 antibody binding
508 using an enzyme linked immunosorbent assay (ELISA). With increasing concentrations of
509 *Pf*MSP2 added to wells coated with AMA1, we found decreased binding of anti-*Pf*AMA1 mAb
510 4G2 and i-body WD34-Fc (mouse Fc) by ELISA (Figure 7D). Concentrations where the
511 *Pf*MSP2 protein was barely detectable above background using an MSP2 mAb were found to
512 be enough to impact on the binding of *Pf*AMA1 antibodies. In contrast, increasing

513 concentrations of the intrinsically disordered MSP4 from *P. falciparum* 3D7 (40 kDa) and the
514 highly structured immunoglobulin domain of neural cell adhesion molecule (NCAM, CD56,
515 16 kDa) recombinant proteins did not impact on binding of anti-*Pf*AMA1 antibodies to
516 recombinant AMA1 (Supplementary Figure 6). By looking at the impacts of removing *Pf*MSP2
517 from the merozoite surface, or adding this protein in to recombinant assays, these data provide
518 additional support that inhibitory antibodies targeting *Pf*AMA1 bind at a higher rate in the
519 absence of *Pf*MSP2.

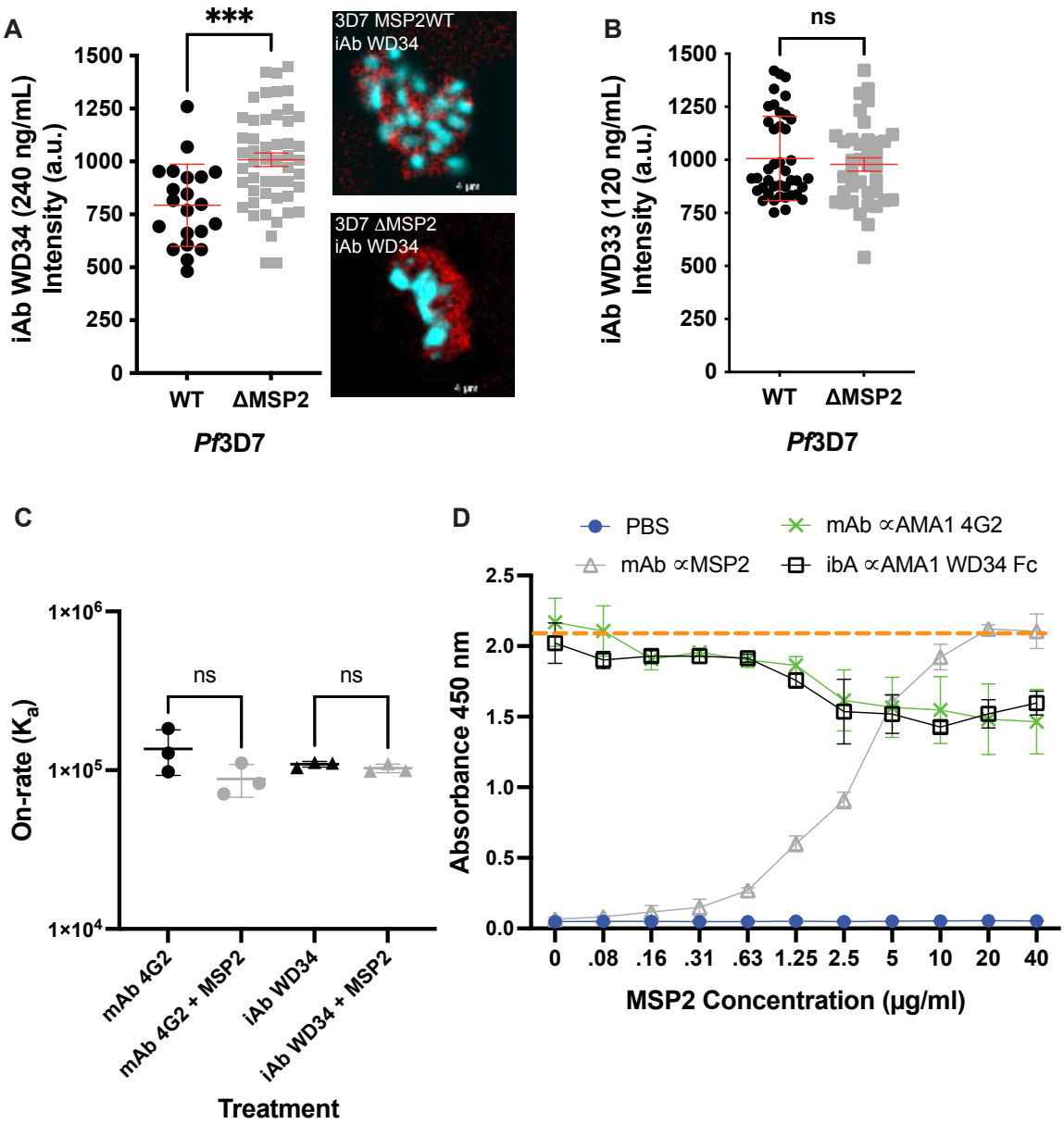

520

521 **Figure 7.** Quantitative fluorescence microscopy to assess whether differential binding may
522 explain the increased potency of anti-*Pf*AMA1 invasion-inhibitory antibodies in the absence
523 of *Pf*MSP2. Fluorescence intensity of fluorescently tagged anti-*Pf*AMA1 i-body (ibA) WD34-

524 mCherry **(A)** and WD33-eGFP **(B)** for both *Pf*3D7 WT and *Pf*3D7 ΔMSP2, with a
525 representative image for i-body WD34-mCherry. Nucleus in blue, i-body signal in red. Scale
526 bar = 4 µm. Two independent experiments were performed with significance determined by
527 unpaired t-test with $p < 0.05$ deemed significant. The lower overall mCherry signal required a
528 higher antibody concentration (240 ng/mL) to have a comparable intensity measure to the
529 eGFP tagged antibody (120 ng/mL) for *Pf*3D7 WT merozoites. **(C)** Read-out of the Surface
530 plasmon resonance (SPR) antibody on-rate (association constant) for anti-*Pf*AMA1 mAb 4G2
531 and i-body WD34-Fc (mouse Fc) binding to *Pf*AMA1 in the presence or absence of *Pf*MSP2
532 protein. Data represents the mean of 3 experiments with significance determined by unpaired
533 t-test with $p < 0.05$ deemed significant. **(D)** ELISA based assessment of the anti-*Pf*AMA1 mAb
534 4G2 and i-body WD34-Fc antibody binding levels to recombinant *Pf*3D7 AMA1 in the
535 presence or absence of recombinant *Pf*3D7 MSP2. PBS control demonstrates background
536 fluorescence. Dashed orange line provides a guide for peak absorbance levels. Anti-*Pf*MSP2
537 mAb shows increasing concentrations of *Pf*MSP2 protein results in decreased binding of mAb
538 4G2 and i-body WD34-Fc. Data represents the mean of 3 experiments and error bars are ±S.D.

539

540 **Discussion**

541 Despite decades of research and interest, the function of most merozoite surface proteins
542 remains unclear and targeting merozoite antigens in vaccine development has not achieved
543 high efficacy in clinical trials. Additionally, it has generally proven difficult to generate highly
544 inhibitory antibodies through vaccination with merozoite antigens. *Pf*MSP2 is one of the most
545 abundant proteins on the merozoite surface, has shown promise as a vaccine candidate and is
546 an established target of protective cytophilic antibodies (Boyle et al., 2015; Genton et al., 2002;
547 McCarthy et al., 2011; Osier et al., 2014, 2010). However, its function remains unclear. Our
548 findings here suggest that *Pf*MSP2 does not have an essential role in invasion *in vitro*, but can
549 modulate the sensitivity of merozoites to inhibitory antibodies targeting other antigens.

550 Despite its abundance on the merozoite surface and previous work suggesting a role in RBC
551 invasion, we found merozoites invade normally in the absence of this protein after gene
552 deletion. This does not exclude a role for *Pf*MSP2 *in vivo* where there are additional pressures,
553 such as immune-effector mechanisms and flow dynamics, on merozoite invasion. However,
554 given we have knocked-out *Pf*MSP2 from two different *P. falciparum* isolates, our findings do
555 not currently support a major role for *Pf*MSP2 in the mechanics of merozoite invasion. Thus,

556 it appears that the function of the two most abundant proteins on the merozoite surface,
557 *Pf*MSP1 (Das et al., 2015; Kals et al., 2024) and *Pf*MSP2, are not directly linked to merozoite
558 binding to the RBC and subsequent invasion. Deletion of MSP2 did lead to significant changes
559 in the expression of several genes, but there were no proteins with a clear link to merozoite
560 invasion and the biological relevance of these changes is not currently understood and requires
561 future investigation.

562 Both rabbit polyclonal and mouse monoclonal anti-*Pf*AMA1 antibodies tested were
563 consistently more inhibitory in the absence of *Pf*MSP2. Of the two *Pf*AMA1 targeting i-bodies
564 tested (Angage et al., 2024), the most potent WD34 was also more potent in the absence of
565 *Pf*MSP2, with this activity increasing significantly with the ~5.6-fold increase in size that
566 occurred upon addition of a human Fc region. Similarly, activity of a nanobody targeting the
567 PCRCR complex protein CSS showed increased potency in the absence of *Pf*MSP2, and again
568 this was increased further with antibody enlargement through addition of an Fc region. These
569 data suggest that *Pf*MSP2 may act to dampen the inhibitory activity of antibodies targeting
570 other antigens on the surface of the merozoite. Such immune dampening (called
571 conformational masking) by intrinsically disordered proteins, or protein regions, of host-cell
572 invasion related proteins has recently been demonstrated by modelling and gene-editing studies
573 in the viral pathogens HIV and HCV, respectively (Li et al., 2024; Stejskal et al., 2022). These
574 studies, along with our demonstration of increase antibody inhibitory efficacy with loss of the
575 intrinsically disordered *Pf*MSP2, support that this may be a widespread approach used by
576 pathogens to protect important protein functional sites from inhibitory antibodies.

577 A role in immune evasion has previously been suggested for *Pf*MSP2 and speculatively an
578 alternate explanation for the sensitisation observed is that this protein may shield key *Pf*AMA1
579 epitopes from antibody inhibition. For the *P. falciparum* 3D7 line, we found that *Pf*MSP2
580 knock-out led to higher *Pf*AMA1 binding as measured by increased fluorescence intensity for
581 the mCherry tagged i-body WD34 in the absence of *Pf*MSP2. Using a solid-phase model and
582 titrating recombinant *Pf*MSP2, we found that increasing concentrations of *Pf*MSP2 reduced
583 binding of an anti-*Pf*AMA1 mAb and i-body, even at concentrations where *Pf*MSP2 was not
584 detectable itself by antibodies. These data support that the presence of *Pf*MSP2 may reduce
585 antibody access (masking) to important invasion proteins exposed on the merozoites surface.
586 However, we acknowledge that the antibody-binding assays used (immunofluorescence assays,
587 SPR, ELISA) might not be sensitive enough to observe all potential changes in binding,
588 temporal changes when binding epitopes are exposed or differences in avidity that could lead

589 to increased antibody potency during the course of parasite invasion and growth, and these
590 factors may also contribute. Future studies of the merozoite surface and interactions between
591 proteins may help decipher in full how *Pf*MSP2 is protecting essential merozoite antigens from
592 invasion inhibitory antibody activity and reveal strategies for enhanced vaccine design.

593 Our observation that loss of *Pf*MSP2 potentiates the invasion-inhibitory activity of antibodies
594 targeting other antigens opens an additional avenue for vaccine development, such as targeting
595 *Pf*MSP2 to interfere with its potential role in immune evasion and thus potentiating antibodies
596 against other merozoite antigens. Additionally, our results suggest that vaccines based on
597 *Pf*AMA1 may need to be designed to specifically avoid the effect of *Pf*MSP2 modulating
598 inhibitory antibodies, such as focussing on specific epitopes or structural features. To date,
599 vaccines based on AMA1 have failed to achieve substantial efficacy (Sagara et al., 2009;
600 Sheehy et al., 2012; Thera et al., 2011). We can speculate that one possible protective
601 mechanism of action of the Combination B vaccine (Genton et al., 2002; McCarthy et al.,
602 2011), which combined *Pf*MSP2, *Pf*MSP1 and *Pf*RESA, could be that the inhibitory activity
603 of vaccine-induced antibodies raised against *Pf*MSP2 were then able to potentiate the activity
604 of antibodies targeting other antigens, potentially *Pf*MSP1 which was also a target of the
605 vaccine. Here we show consistent potency improvement with *Pf*MSP2 knock-out for growth
606 inhibitory rabbit, mouse monoclonal and i-body antibodies targeting *Pf*AMA1, as well as
607 demonstrate improved activity for and Fc-tagged nanobody targeting *Pf*CSS, indicating that
608 these are not outlier results from a single antibody or antibody type. However, increased
609 antibody potency was not shared across all antibodies tested, possibly because the specific
610 function or localisation of a target protein, the region that an antibody binds to or the functional
611 activity (or lack thereof) of an antibody may all play a role in determining whether loss of
612 *Pf*MSP2 can potentiate growth inhibitory activity. Further investigation using the parasite lines
613 developed in this study and a wider panel of antibodies that target different stages of the
614 merozoite invasion process could shed more light on this potentially novel mechanism of
615 vaccine derived antibody efficacy.

616 The results of this study and work done by Escalante et al. (2022) demonstrate that MSP2-like
617 sequences are found in the avian malarias *P. galinaceum* and *P. relictum*, which differs from
618 the fields previous understanding that *Pf*MSP2 arose in the *Laverania* lineage of malaria
619 parasites. This observation indicates that MSP2 was likely present in the ancestral malaria
620 parasite before being lost in primate and rodent *Plasmodium* spp. Further insights into the
621 evolution and loss of *Pf*MSP2 are likely to be found with additional whole genome sequences

622 of bird and lizard malaria species. The presence of *msp2*-like sequences in some avian
623 *Plasmodium* species and *Laverania* suggest a retention of *msp2* sequences in the *Laverania*
624 which indicates an important role for MSP2 for these parasites. Indeed, our amino acid and
625 structural prediction level comparison demonstrates that much of the protein properties
626 conserved in the *Laverania* MSP2s are also recognisable, and in many cases conserved, in the
627 avian malaria MSP2s, despite 10 million years of evolutionary divergence. This suggests that
628 having an MSP2-like protein is beneficial for these parasites with very different hosts.
629 However, CRISPR-Cas9 gene editing used in this work has shown that, in contrast to previous
630 work, *Pf*MSP2 is not essential for *P. falciparum* blood stage parasite growth *in vitro*. Our
631 findings raise the possibility that the retention of *Pf*MSP2 in the *Laverania*, and by association
632 potentially the avian malaria parasites, may be linked to its apparent capacity to modulate the
633 impact of antibodies against other merozoite surface-exposed antigens, rather than through a
634 direct mechanistic role in host-cell invasion. If MSP2 was to fulfill such a role in the *Laverania*
635 and avian malaria parasites, it raises the question of whether a similar protective system exists
636 in other *Plasmodium* spp. and what the key protein/s are that fulfil this role in these parasites.

637 The *Pf*3D7 MSP2 and *Pf*Dd2 MSP2 lines developed in this study will provide useful reagents
638 for investigating the potential of targeting a single, or both, *Pf*MSP2 allelic types with vaccines
639 that elicit different immune responses. These parasites could also be used to explore whether
640 vaccine-induced antibodies against other merozoite antigens could also be potentiated if any
641 immune evasion mechanism provided by *Pf*MSP2 is removed. This may be achievable with a
642 combination vaccine or through targeting an epitope of another merozoite vaccine candidate
643 that is not protected by *Pf*MSP2. Such information, investigated using the *Pf*MSP2 knock-out
644 parasites developed in this study, could be useful in prioritising vaccine candidates, specific
645 epitopes and combinations that target the merozoite.

646

647 **Conclusion**

648 Advancements in gene-editing techniques in *P. falciparum* have allowed us to show for the
649 first time, and contrary to previous work, that *Pf*MSP2 is not essential for *P. falciparum* growth
650 *in vitro*. Instead, we present a new concept that MSP2 can modulate the activity of invasion-
651 inhibitory antibodies and may have evolved for this purpose. It is possible that other merozoite
652 surface proteins may have similar roles and should be investigated in future studies. Our
653 observation that loss of *Pf*MSP2 potentiates the inhibitory activity of antibodies targeting other

654 merozoite surface exposed proteins reveals a new avenue to explore in vaccine development
655 by blocking or bypassing this function to improve the activity of vaccines targeting these
656 antigens.

657

658 **Materials and Methods**

659

660 **Bioinformatic analysis of *Pf*MSP2, *Pf*MSP4 and *Pf*MSP5 like proteins in *Plasmodium* spp.**

661 The PlasmoDB database (Aurrecoechea et al., 2009) was used to identify in the available
662 *Plasmodium* genomes the region between Adenylosuccinate lyase (PF3D7_0206700) and a
663 conserved protein of unknown function (PF3D7_0207100) where *Pf*MSP2, *Pf*MSP4 and
664 *Pf*MSP5 are localised in *P. falciparum*. All annotated MSP2, MSP4 and MSP5 protein
665 sequences were downloaded. Translated sequences of unannotated genes and putative
666 annotations in this region were also downloaded and aligned using the MUSCLE alignment
667 tool MEGA11: Molecular Evolutionary Genetics Analysis version 11 (Tamura et al., 2021) or
668 the Geneious Prime 2019.2.1 MUSCLE alignment tool (Biomatters Ltd.) and determined to be
669 MSP2, MSP4 or MSP5 based on sequence similarity in the conserved regions of these genes.
670 A BLAST (NCBI) search with the N-terminal and C-terminal conserved regions of MSP2 was
671 also performed to capture any sequences missed by the above approach. A maximum likelihood
672 phylogenetic tree of identified MSP2 sequences was generated using the default maximum
673 likelihood settings of MEGA11 with 500 bootstraps and the *P. gallinaceum* MSP2 as an
674 outgroup.

675

676 **Modelling of MSP structure across *Plasmodium* spp. using Alpha-fold**

677 In order to obtain models of the 3-dimensional protein structures of MSP2 for *P. falciparum*,
678 *P. reichenowi*, *P. billcollinsi*, *P. adleri*, *P. relictum* and *P. gallinaceum*, we first removed the
679 predicted N-terminal signal sequences and C-terminal GPI anchor sequence. The resulting
680 sequences were submitted to AlphaFold2 (Jumper et al., 2021). The resulting models were
681 subsequently analysed and visualised using PyMOL 2.4.0 (Schrödinger, USA).

682

683 **Culture and synchronisation of *P. falciparum***

684 *Plasmodium falciparum* 3D7 and Dd2 was cultured in RPMI-HEPES media (Gibco) containing
685 0.5% Albumax ll (Gibco), 25 μM Gentamicin (Gibco), 367 μM hypoxanthine (Sigma Aldrich),
686 2 mM L-Glutamax (Gibco), 0.17% sodium bicarbonate (Sigma Aldrich) and O positive human
687 red blood cells (Lifeblood, Australia) at 3% parasitemia, 3% haematocrit. Cultures were grown
688 at 37°C under 1% oxygen, 5% CO_2 (BOC gas), in a humidified chamber. For gene-edited lines,
689 WR99210 (Jakobus Pharmaceuticals) was added to culture media. Sorbitol lysis (5%) (Sigma
690 Aldrich) to select for ring-stage parasites, Percoll Plus (Sigma Aldrich) selection of late-stage
691 parasites and heparin treatment (Pfizer) (Boyle et al., 2010b) were used to maintain
692 synchronicity of parasite cultures.

693

694 **Generation of *Pf*MSP2 knockout line using CRISPR Cas9**

695 Briefly, a flank region incorporating the 5' region upstream of *Pf*MSP2, the first 44 amino
696 acids of the protein, and a flank of the region immediately 3' of *Pf*MSP2 was inserted into the
697 pCC1 plasmid by restriction enzyme cloning. A 20 bp guide sequence was designed using
698 EuPaGDT (Peng and Tarleton, 2015), annealed and inserted in the pUF_Cas9 plasmid by
699 infusion cloning (Takara Bio). pUF_Cas9 guide plasmid (20 μg) and pCC1 *Pf*MSP2 repair
700 plasmid (60 μg) was transfected directly into *P. falciparum* schizonts. Early schizonts were
701 purified using a 70% percoll gradient and treated for 4 hrs with compound 1 (Taylor et al.,
702 2010) at 2 μM. After incubation treated schizonts were washed twice and left shaking for 20
703 minutes before pelleting and resuspension in Complete Cytomix (plasmids plus 0.895% KCl,
704 0.0017% $CaCl_2$, 0.076% EGTA, 0.102% $MgCl_2$, 0.0871% K_2HPO_4, 0.068% KH_2PO_4, 0.708%
705 HEPES). Schizonts were electroporated in 0.2 cm cuvettes (Biorad) at 800 V and 25 μF.
706 Electroporated schizonts were mixed with warmed media and fresh RBCs and shaken to
707 promote invasion for 20 minutes after which they were placed in a culture dish. Transfected
708 parasites were then treated with WR99210 to select for integration of the hDHFR drug selection
709 cassette and MSP2 knock-out.

710 To confirm integration gDNA was collected by saponin lysis of schizont stage parasite culture
711 and gDNA extracted using the PureLink Genomic DNA Mini Kit (Invitrogen) as per
712 manufacturer's instructions. Integration of the *Pf*MSP2 knockout construct into a portion of
713 parasites was confirmed by PCR (Supplementary Table 1). Once confirmed cultures were
714 cycled on and off WR99210 (Jakobus Pharmaceuticals) and 1 μM 5FC (Sigma Aldrich) to

715 select for integrated parasites no longer expressing the guide plasmid. Limited dilution cloning
716 was then performed to obtain parasite clones which had integrated the knockout construct.

717

718 **Western blotting to detect *Pf*MSP2**

719 Synchronised schizonts were harvested and the RBCs lysed by saponin. Briefly ~10 mL
720 schizont (38-44 hrs) culture was lysed on ice for 10 minutes with 0.15% w/v saponin before
721 pelleting by centrifugation and washing once in 0.075% w/v saponin followed by three washes
722 in PBS containing protease inhibitors (CØmplete, Roche). Saponin treated schizont pellets
723 were treated with DNAsel (Qiagen) for 10 minutes at room temperature before resuspension
724 in reducing sample buffer (0.125 M Tris-HCL, 4% SDS, 20% glycerol, 10% beta-
725 mercaptoethanol and 0.002% bromophenol blue). Proteins were separated by size using SDS-
726 PAGE 4-12% Bis-Tris Gels (Bolt, Invitrogen) at 110V for 80 minutes before transfer to a
727 nitrocellulose membrane (iBlot, Invitrogen) at 20V for 7 minutes. Blots were blocked from 1
728 hr to overnight in 3% skim milk PBS (Sigma Aldrich) before incubation with primary
729 antibodies (1/75000 mouse 2F2 anti-*Pf*MSP2 3D7 (Supplementary Table 2; (Adda et al.,
730 2012)) and 1/75000 rabbit anti-*Plasmodium* aldolase (Abcam) or 1/75000 rabbit anti-FC27 and
731 1/10000 mouse anti- EXP2 (a gift of Paul Gilson, Burnet Institute, Melbourne) for 1- 2 hrs.
732 IRDye 800CW goat anti-mouse (1/4000, LI-COR Biosciences) or IRDye 680RD goat anti-
733 rabbit (1/4000, LI-COR Biosciences) secondary antibodies were used for detection on the
734 Odyssey Infrared imaging system (LI-COR Biosciences). Quantification was performed using
735 Image Studio Lite 5.2.5 (LI-COR Biosciences).

736 **Quantification of parasite expansion rate and invasion inhibition**

737 Potential growth defects resulting from gene editing was assessed by flow cytometry. The
738 initial parasitemia of cultures was determined by flow cytometry and then measured again after
739 the 50 µL cultures in 96 well plates were maintained under standard (still) or shaking (50 rpm)
740 conditions for 48 hrs or 96 hrs of growth. To determine parasitemia by flow cytometry
741 Ethidium Bromide (10 µg/mL BioRad) was added to 50 µL of 1% haematocrit culture for 30
742 mins to allow for staining of parasite DNA. The stain was washed off and wells resuspended
743 in 200µL of PBS. Data was collected on a BD Accuri C6 Plus Flow Cytometer (BD
744 Biosciences) and analysed on FlowJo (FlowJo LLC). Briefly, forward scatter and side scatter
745 was used to determine the RBC population. From this population infected RBCs were gated

746 on as highly fluorescent in the PE channel. Final parasitemia was compared back to initial
747 parasitemia to determine the fold increase in parasitemia for each line.

748 To examine the invasion inhibitory effect of antibodies (Supplementary Table 2), 5 μL of
749 potential inhibitor was mixed with 45 μL of 0.2% schizont parasitemia at 1% haematocrit for
750 96 hrs before end parasitemia was determined by flow cytometry. Data is displayed as %
751 Growth of media only controls for each line.

752 To examine differences in RBC receptor preference RBCs were treated with different enzymes
753 that cleave different residues of RBC receptors which is used as a marker for which RBC
754 receptor/s are preferred by *P. falciparum* (Duraisingh et al., 2003). Infected RBCs at 1% ring
755 stage parasitemia were washed three times in RPMI-HEPES to remove excess protein. Packed
756 RBCs (20 μL) at 1% parasitemia were then resuspended with 5X RBC volume of pre-warmed
757 enzymes at desired concentration (Supplementary Table 3). RBC-enzyme mix was incubated
758 at 37°C for 45 mins with rotation to keep RBCs resuspended. Following incubation, RBCs
759 were washed three times and added to fresh complete media at 1% haematocrit in a U- bottom
760 96 well plate in technical duplicate. Plates were incubated for 72 hrs, sufficient time for *P.*
761 *falciparum* to complete one full cycle of growth and reach trophozoite stage again. Final
762 parasitemia was determined by flow cytometry, as detailed above, and compared to non-treated
763 controls. IC_{50} calculations data was log transformed then a nonliner regression log-(inhibitor)-
764 versus-response curve was calculated with Extra Sum-of-Squares F Test (best-fit $LogIC_{50}$)
765 used to compared IC_{50}s between conditions.

766

767 **Immunofluorescence assay of Wildtype and *Pf*MSP2 KO parasites**

768 Schizonts ~38 hrs old were treated with E64 (Sigma-Aldrich) for 5 hrs to allow development
769 of very mature schizonts desired for imaging. After E64 treatment, parasite cultures were fixed
770 in 4% v/v paraformaledehyde (PFA, Sigma-Aldrich), 0.0075% v/v glutaraldehyde (pH 7.5,
771 Electron Microscopy Sciences) solution for 30 min at room temperature shaking gently. Fixed
772 parasites were washed in 1X PBS and then resuspended in PBS at 1% haematocrit. Coverslips
773 (#1.5H high-precision coverslips, Carl Zeiss, Oberkochen, Germany) were coated in 0.01%
774 Poly-L-lysine (Sigma Aldrich) for 1 hr at room temperature, washed in miliQ water before the
775 fixed parasite culture was allowed to adhere for 1 hr. Cells were permeabilised by 0.1% Triton
776 X-100 PBS for 10 mins before blocking for 1 hr to overnight in 3% BSA 0.05% Tween 20
777 PBS. Primary antibodies were diluted in 1% BSA 0.05% Tween 20 PBS and incubated for 2

778 hrs. Coverslips were washed in 0.05% Tween 20 PBS three times before incubation with the
779 secondary antibody (1/500 goat anti-chicken/mouse/rabbit Alexa Fluor coupled secondary
780 antibodies -488 nm, 594 nm, 647 nm; Life Technologies) for 1 hr. After the secondary antibody
781 was washed off coverslips underwent a secondary fix in 4% v/v PFA, 0.0075% v/v
782 glutaraldehyde for 5 mins. The fixative was washed off and the coverslips dehydrated with
783 sequential 3 min ethanol treatment (70%, 90% and 100%). Coverslips were allowed to dry and
784 mounted with ProLong Gold antifade solution (refractive index 1.4) which contains 4', 6-
785 diamidino-2phenylindole, dihydrochloride (DAPI) (ThermoFisher Scientific) and allowed to
786 set overnight. Imaging was performed on the Zeiss LSM 800 using the Airyscan super-
787 resolution mode (Carl Zeiss, Obekochen, Germany).

788

789 **Live cell microscopic analysis of merozoite RBC invasion**

790 Highly synchronised *Pf*Dd2 and *Pf*Dd2 ΔMSP2 parasites at schizont stages were adjusted to
791 0.25% Haematocrit in complete culture medium. A volume of 200 µL was added to a well of
792 an iBidi 15 µ-Slide 8 well, glass bottom slide (iBidi 80827) and the slide was promptly returned
793 to sit on a prewarmed water block within a gassed box and left to incubate at 37ºC to allow
794 iRBCs to settle. The slide was then transported directly to a prewarmed Nikon TiE microscope
795 with an environmental chamber heated to 37ºC and gas mixture of 1% O_2, 5% CO_2 and 94%
796 nitrogen. Filming was conducted using either a 60X water or 100X oil objective. Differential
797 interference contrast (DIC) imaging was captured at 3 – 3.5 Volts with a camera exposure of
798 60 – 180 milliseconds.

799 Captured footage was processed using the Nikon analysis software (NIS-Elements AR
800 Analysis version 5.21.01) and analysis of the schizont rupture and merozoite invasion events
801 was performed manually. The merozoites which invaded successfully were tracked and
802 attachment time, reorientation time (if obvious), deformation start and end times, the
803 deformation score (Weiss et al., 2015; Wilson et al., 2015), invasion initiation and completion
804 times and echinocytosis start times were recorded.

805

806 **RNA extraction**

807 Highly synchronised cultures were pelleted, resuspended in TriZol (Invitrogen) and incubated
808 for 5 minutes at 37ºC. Chloroform (Sigma Aldrich) was added, mixed and then spun at 12,000g

809 for 30 minutes at 4ºC. Supernatant was collected and mixed with an equal volume of 70%
810 Ethanol and processed using the RNeasy Kit (Qiagen) to extract purified RNA. RNA was
811 DNAse l (Qiagen) treated for 30 mins at room temperature and cleaned up on RNeasy columns
812 according to the manufacturers protocol. Absence of gDNA was checked by qPCR of gDNA
813 with primers (*Pf*SUB1) and DNAse I treatment repeated if necessary.

814

815 **qPCR of gene expression in schizonts**

816 DNAse treated RNA was added to 40 mM dNTPs (Qiagen), 0.4 mg/mL random hexamer
817 (Qiagen) and incubated at 65ºC for 5 mins. After incubation 5x Superscript Buffer (Invitrogen),
818 100 mM DTT (Invitrogen), 40 U/µL RNAseOUT (Invitrogen) and 200 µ/mL Superscript lll
819 Reverse Transcriptase (Invitrogen) was added and cycled 25ºC 5 mins, 50ºC for 60 mins and
820 70ºC for 15 mins. Primers (Supplementary Table 4) were designed to detect *Pf*MSP2, *Pf*MSP4,
821 *Pf*MSP5, *Pf*SUB1 and Fructose Bisphosphate Aldolase as a reference gene (Salanti et al.,
822 2003). qPCR was performed on cDNA from WT and knockout parasites with PowerUp SYBR
823 Green Master Mix (Applied Biosystems) and cycling parameters; 95ºC for 10 mins followed
824 by 40 cycles 95ºC for 15 mins, 60ºC for 14 mins before a dissociation step at 95ºC for 2 mins
825 followed by 60ºC for 2 mins with a 2% ramp to 95ºC for 2 mins on the QuantStudio 7 Flex
826 System (ThermoFisher). qPCR was performed in triplicate for each of the three independent
827 experiments. Change in gene expression in knockout lines compared to WT was quantified by
828 the $2^{-\Delta\Delta Ct}$ method (Livak and Schmittgen, 2001).

829

830 **Differential gene expression in *Pf*MSP2 KO compared to WT schizonts**

831 RNA sequencing of the schizont stage transcriptome of *Pf*3D7 MSP2 KO and *Pf*3D7 WT was
832 performed using the Illumina total RNA with Ribo Zero plus for library preparation and
833 sequenced on the NovaSeq 6000 platform (Victorian Clinical Genetics Services) with 2x150
834 bp paired end reads (Supplementary Table 5). Reads were aligned to the *Pf*3D7 reference
835 genome (PlasmoDB v61) using STAR aligner (Dobin et al., 2013). Reads were called using
836 Rsubread FeatureCounts (Liao et al., 2014) with reads counted by CDS and summarised by
837 gene. Differential gene analysis was performed with DESeq2 (Love et al., 2014) and visualized
838 in R studio using ggplots2 (Wickham, 2016). MSP2 RNASeq data is available at ArrayExpress
839 through accession number E-MTAB-15427.

840

841 **Quantitative Immunofluorescence assay**

842 Synchronous *Pf*3D7 MSP2 KO and *Pf*3D7 WT parasite cultures were treated with ML10
843 (Ressurreição et al., 2020) to allow mature schizonts to develop. Thin blood smears were then
844 made and fixed in 100%, -20°C methanol for 5 mins. Blocking of smears was performed in 1%
845 BSA PBS, then fluorophore conjugated WD34 (240 ng/mL) and WD33 (120 ng/mL) i-bodies
846 (Angage et al., 2024) in 1% BSA PBS were added and incubated at room temperature for 1 hr.
847 Smears were then washed, ethanol dehydrated and a coverslip mounted (ProLong Diamond
848 Antifade mountant with DAPI (refractive index 1.47, ThermoFisher Scientific)) and allowed
849 to cure for 48 hrs at room temperature. Fluorescence images were acquired using an Olympus
850 FV3000 confocal microscope equipped with a 100x oil objective (NA 1.4). Quantification of
851 parasite associated fluorescence was performed using a modified image analysis pipeline
852 (Liffner et al., 2020) implemented in Imaris™ (9.9 version) where non-specific background
853 fluorescence was removed using rolling ball background subtraction and a thresholding
854 algorithm applied to the image to generate binary masks, separating objects exceeding the
855 threshold (putative parasites) from the background. Binary masks were further refined to
856 exclude objects smaller or larger than a defined size range (< 3 μm and > 15 μm),
857 corresponding to the expected size of AMA i-body stained schizonts. Following segmentation
858 the surface area containing antibody signal were calculated and these values compared between
859 *Pf*3D7 MSP2 KO and *Pf*3D7 WT parasites.

860

861 **Surface Plasmon Resonance (SPR) Assay**

862 Surface plasmon resonance (SPR) was employed to determine the association rate constant
863 (K_a) of AMA1-antibody interactions in the presence of MSP2 using the Biacore T200 system
864 (Cytiva). Flow cells 1, 2, and 3 were activated for 14 minutes using a 1:1 mixture of 0.1 M N-
865 hydroxysuccinimide (NHS) and 0.4 M N-(3-dimethylaminopropyl)-N'-ethylcarbodiimide
866 hydrochloride (EDC) at a flow rate of 5 μL/min. Flow cell one was immobilised with bovine
867 serum albumin (BSA) to serve as a reference surface. AMA1 was immobilised at a
868 concentration of 80 μg/mL in 10 mM sodium acetate (pH 4.5) to achieve a surface density of
869 1000 response units (RU) on flow cells Two and three. MSP2 was co-immobilised in flow
870 cell three to a surface density of 2000 RU. All surfaces were subsequently blocked with a 7-
871 minute injection of 1 M ethanolamine (pH 8.0). Purified antibodies were prepared in PBS
872 containing 0.005% Tween-20 (pH 7.4) and injected over the flow cells at a flow rate of 60

873 µL/min at 25°C. Single-cycle kinetics, using a bivalent analyte model, was applied to analyse
874 the interactions.

875

876 **Enzyme-Linked Immunosorbent Assay (ELISA)**

877 ELISAs to evaluate the effect of MSP2 on the binding of AMA1-specific antibodies were
878 carried out in a volume of 100 µL per well, either at room temperature for 1 hr or overnight
879 at 4°C. All washing steps consisted of three washes with PBS containing 0.1% Tween-20
880 (PBS-T). Nunc Maxisorp plates (Thermo Fisher Scientific, USA) were coated with AMA1
881 at a concentration of 0.8 µg/mL, followed by washing and subsequent coating with
882 increasing concentrations of recombinant HIS-tagged *Pf*MSP2, HIS-tagged *Pf*MSP4 or HIS-
883 tagged NCAM. Wells were then blocked with 5% (w/v) skim milk in PBS and then
884 incubated for 1 hr at room temperature with one of mouse Fc-conjugated WD34 anti-AMA1
885 i-body (Angage et al., 2024), mouse monoclonal anti-AMA1 antibody (mAb) 4G2 (Kocken
886 et al., 1998), anti-MSP2 mAb 9G8 (Adda et al., 2012), anti-HIS antibody (Sigma Aldrich) to
887 detect *Pf*MSP4 or anti-NCAM antibody (21H5, (Griffiths et al., 2016)) at a concentration of
888 2.5 µg/mL. The primary antibody was washed off and the HRP-conjugated secondary
889 antibody (1:5000, Sigma Aldrich) was then applied for 1 hr at room temperature before
890 washing. For signal development to detect bound primary antibodies, wells were incubated
891 with 1-Step™ Ultra TMB-ELISA Substrate Solution (Thermo Fisher Scientific, USA)
892 according to the manufacturers instructions. The reaction was stopped by adding 1 M
893 sulfuric acid, and the absorbance at 450 nm was measured using a microplate reader.

894

895 **Statistical Analysis**

896 Three independent experiments were performed for all experiments in technical duplicate,
897 unless otherwise stated. Data was graphed and statistical tests performed in Prism GraphPad
898 v9 or R.

899

900

901 **Acknowledgements**

902 The authors would like to thank Prof Alan Cowman, Dr Stephen Scally and Jennifer Thompson
903 (WEHI, Melbourne) for provision of PCRCR complex antibodies. Assoc Prof Paul Gilson

904 (Burnet Institute, Melb) for EXP2 and MSP1 antibodies. Dr Chris MacRaild (Monash
905 University) for helpful discussion. Dr Adam Thomas for the *Pf*MSP4 protein (Burnet Institute).
906 Dr Sonja Frölich (the University of Adelaide) for assistance on quantitative
907 immunofluorescence assays and Adelaide Microscopy for training and use of microscopy
908 instruments. We thank Lifeblood, Australia, for provision of RBCs. DWW was supported by
909 a Hospital Research Foundation (C-MCF-52-2019) and Australian Research Council
910 (FT240100420) Future Fellowship. DWW and JGB by a Hospital Research Foundation
911 Collaborative Grant (S-03-EOI-2021). JGB was supported by the National Health and Medical
912 Research Council of Australia (Research Fellowship and Investigator Grant to JGB, Australian
913 Centre for Research Excellence in Malaria Research). IGH and JC were supported by an
914 Australian Research Council RTP scholarship. The Burnet Institute is supported by the
915 NHMRC for Independent Research Institutes Infrastructure Support Scheme and the Victorian
916 State Government Operational Infrastructure Support.

917

918 **Author Contributions**

919 Conceived and designed the experiments: DWW, IGH, JC, JGB, DA, MF, RA. Performed the
920 experiments and phylogenetic analysis: IGH, JC, KHL, OR, DA, KRT, NB. Analysed the data:
921 IGH, DWW, JC, KHL, OR, DA, MF. Provided key discussions on PfMSP2 and/or key
922 reagents: RA, MF, DA. Paper writing: DWW, JC, IGH, JGB with critical input from RA, MF,
923 DA, OR, KRT and based on the PhD thesis of IGH.

924

925 **Competing Interests**

926 M.F. is the founding chief scientist and a shareholder in AdAlta Ltd., and R.F.A. is also a
927 shareholder in AdAlta. The other authors have declared no competing interests.

928

929 **References**

930 Adda, C.G., MacRaild, C.A., Reiling, L., Wycherley, K., Boyle, M.J., Kienzle, V., Masendycz,
931 P., Foley, M., Beeson, J.G., Norton, R.S., Anders, R.F., 2012. Antigenic characterization

932 of an intrinsically unstructured protein, Plasmodium falciparum merozoite surface protein
933 2. Infect Immun 80, 4177–4185. https://doi.org/10.1128/IAI.00665-12

934 Adda, C.G., Murphy, V.J., Sunde, M., Waddington, L.J., Schloegel, J., Talbo, G.H., Vingas,
935 K., Kienzle, V., Masciantonio, R., Howlett, G.J., Hodder, A.N., Foley, M., Anders, R.F.,
936 2009. Plasmodium falciparum merozoite surface protein 2 is unstructured and forms
937 amyloid-like fibrils. Mol Biochem Parasitol 166, 159–171.
938 https://doi.org/10.1016/j.molbiopara.2009.03.012

939 Alanine, D.G.W., Quinkert, D., Kumarasingha, R., Mehmood, S., Donnellan, F.R., Minkah,
940 N.K., Dadonaite, B., Diouf, A., Galaway, F., Silk, S.E., Jamwal, A., Marshall, J.M.,
941 Miura, K., Foquet, L., Elias, S.C., Labbé, G.M., Douglas, A.D., Jin, J., Payne, R.O.,
942 Illingworth, J.J., Pattinson, D.J., Pulido, D., Williams, B.G., de Jongh, W.A., Wright, G.J.,
943 Kappe, S.H.I., Robinson, C. V, Long, C.A., Crabb, B.S., Gilson, P.R., Higgins, M.K.,
944 Draper, S.J., 2019. Human Antibodies that Slow Erythrocyte Invasion Potentiate Malaria-
945 Neutralizing Antibodies. Cell 178, 216-228.e21.
946 https://doi.org/10.1016/j.cell.2019.05.025

947 Anders, R.F., Adda, C.G., Foley, M., Norton, R.S., 2010. Recombinant protein vaccines against
948 the asexual blood-stages of Plasmodium falciparum. Hum Vaccin 6, 39–53.
949 https://doi.org/10.4161/hv.6.1.10712

950 Angage, D., Chmielewski, J., Maddumage, J.C., Hesping, E., Caiazzo, S., Lai, K.H., Yeoh,
951 L.M., Menassa, J., Opi, D.H., Cairns, C., Puthalakath, H., Beeson, J.G., Kvansakul, M.,
952 Boddey, J.A., Wilson, D.W., Anders, R.F., Foley, M., 2024. A broadly cross-reactive i-
953 body to AMA1 potently inhibits blood and liver stages of Plasmodium parasites. Nat
954 Commun 15, 7206. https://doi.org/10.1038/s41467-024-50770-7

955 Aurrecoechea, C., Brestelli, J., Brunk, B.P., Dommer, J., Fischer, S., Gajria, B., Gao, X.,
956 Gingle, A., Grant, G., Harb, O.S., Heiges, M., Innamorato, F., Iodice, J., Kissinger, J.C.,
957 Kraemer, E., Li, W., Miller, J.A., Nayak, V., Pennington, C., Pinney, D.F., Roos, D.S.,
958 Ross, C., Stoeckert, J.C.J., Treatman, C., Wang, H., 2009. PlasmoDB: a functional
959 genomic database for malaria parasites. Nucleic Acids Res 37, D539–D543.
960 https://doi.org/10.1093/nar/gkn814

961 Bannister, L.H., Mitchell, G.H., Butcher, G.A., Gennis, E.D., Cohen, S., 1986. Structure and
962 development of the surface coat of erythrocytic merozoites of Plasmodium knowlesi. Cell
963 Tissue Res 245, 281–290.

964 Baum, J., Maier, A.G., Good, R.T., Simpson, K.M., Cowman, A.F., 2005. Invasion by P.
965 falciparum Merozoites Suggests a Hierarchy of Molecular Interactions. PLoS Pathog 1,
966 e37.

967 Beeson, J.G., Drew, D.R., Boyle, M.J., Feng, G., Fowkes, F.J.I.I., Richards, J.S., 2016.
968 Merozoite surface proteins in red blood cell invasion, immunity and vaccines against
969 malaria. FEMS Microbiol Rev 40, 343–372. https://doi.org/10.1093/femsre/fuw001

970 Beeson, J.G., Kurtovic, L., Dobaño, C., Opi, D.H., Chan, J.-A., Feng, G., Good, M.F., Reiling,
971 L., Boyle, M.J., 2019. Challenges and strategies for developing efficacious and long-
972 lasting malaria vaccines. Sci Transl Med 11.
973 https://doi.org/10.1126/scitranslmed.aau1458

974 Black, C.G., Barnwell, J.W., Huber, C.S., Galinski, M.R., Coppel, R.L., 2002. The
975 Plasmodium vivax homologues of merozoite surface proteins 4 and 5 from Plasmodium
976 falciparum are expressed at different locations in the merozoite. Mol Biochem Parasitol
977 120, 215–224. https://doi.org/https://doi.org/10.1016/S0166-6851(01)00458-3

978 Böhme, U., Otto, T.D., Cotton, J.A., Steinbiss, S., Sanders, M., Oyola, S.O., Nicot, A., Gandon,
979 S., Patra, K.P., Herd, C., Bushell, E., Modrzynska, K.K., Billker, O., Vinetz, J.M., Rivero,
980 A., Newbold, C.I., Berriman, M., 2018. Complete avian malaria parasite genomes reveal
981 features associated with lineage-specific evolution in birds and mammals. Genome Res
982 28, 547–560. https://doi.org/10.1101/gr.218123.116

983 Boyle, M.J., Langer, C., Chan, J.-A., Hodder, A.N., Coppel, R.L., Anders, R.F., Beeson, J.G.,
984 2014. Sequential Processing of Merozoite Surface Proteins during and after Erythrocyte
985 Invasion by Plasmodium falciparum. Infect Immun 82, 924–936.
986 https://doi.org/10.1128/IAI.00866-13

987 Boyle, M.J., Reiling, L., Feng, G., Langer, C., Osier, F.H., Aspeling-Jones, H., Cheng, Y.S.,
988 Stubbs, J., Tetteh, K.K.A., Conway, D.J., McCarthy, J.S., Muller, I., Marsh, K., Anders,
989 R.F., Beeson, J.G., 2015. Human antibodies fix complement to inhibit plasmodium
990 falciparum invasion of erythrocytes and are associated with protection against malaria.
991 Immunity 42, 580–590. https://doi.org/10.1016/j.immuni.2015.02.012

992 Boyle, M.J., Richards, J.S., Gilson, P.R., Chai, W., Beeson, J.G., 2010a. Interactions with
993 heparin-like molecules during erythrocyte invasion by Plasmodium falciparum
994 merozoites. Blood 115, 4559–4568. https://doi.org/10.1182/blood-2009-09-243725

995 Boyle, M.J., Wilson, D.W., Richards, J.S., Riglar, D.T., Tetteh, K.K.A., Conway, D.J., Ralph,
996 S.A., Baum, J., Beeson, J.G., 2010b. Isolation of viable Plasmodium falciparum
997 merozoites to define erythrocyte invasion events and advance vaccine and drug
998 development. Proc Natl Acad Sci U S A 107, 14378–14383.
999 https://doi.org/10.1073/pnas.1009198107

1000 Coley, A.M., Gupta, A., Murphy, V.J., Bai, T., Kim, H., Anders, R.F., Foley, M., Batchelor,
1001 A.H., 2007. Structure of the Malaria Antigen AMA1 in Complex with a Growth-
1002 Inhibitory Antibody. PLoS Pathog 3, e138.

1003 Cowman, A.F., Tonkin, C.J., Tham, W.-H., Duraisingh, M.T., 2017. The Molecular Basis of
1004 Erythrocyte Invasion by Malaria Parasites. Cell Host Microbe 22, 232–245.
1005 https://doi.org/10.1016/j.chom.2017.07.003

1006 Crosnier, C., Bustamante, L.Y., Bartholdson, S.J., Bei, A.K., Theron, M., Uchikawa, M.,
1007 Mboup, S., Ndir, O., Kwiatkowski, D.P., Duraisingh, M.T., Rayner, J.C., Wright, G.J.,
1008 2011. Basigin is a receptor essential for erythrocyte invasion by Plasmodium falciparum.
1009 Nature 480, 534–537. https://doi.org/10.1038/nature10606

1010 Das, S., Hertrich, N., Perrin, A.J., Withers-Martinez, C., Collins, C.R., Jones, M.L.,
1011 Watermeyer, J.M., Fobes, E.T., Martin, S.R., Saibil, H.R., Wright, G.J., Treeck, M., Epp,
1012 C., Blackman, M.J., 2015. Processing of Plasmodium falciparum Merozoite Surface
1013 Protein MSP1 Activates a Spectrin-Binding Function Enabling Parasite Egress from
1014 RBCs. Cell Host Microbe 18, 433–444. https://doi.org/10.1016/j.chom.2015.09.007

1015 Datoo, M.S., Dicko, A., Tinto, H., Ouédraogo, J.B., Hamaluba, M., Olotu, A., Beaumont, E.,
1016 Ramos Lopez, F., Natama, H.M., Weston, S., Chemba, M., Compaore, Y.D., Issiaka, D.,
1017 Salou, D., Some, A.M., Omenda, S., Lawrie, A., Bejon, P., Rao, H., Chandramohan, D.,
1018 Roberts, R., Bharati, S., Stockdale, L., Gairola, S., Greenwood, B.M., Ewer, K.J., Bradley,
1019 J., Kulkarni, P.S., Shaligram, U., Hill, A.V.S., Mahamar, A., Sanogo, K., Sidibe, Y.,
1020 Diarra, K., Samassekou, M., Attaher, O., Tapily, A., Diallo, M., Dicko, O.M., Kaya, M.,
1021 Maguiraga, S.O., Sankare, Y., Yalcouye, H., Diarra, S., Niambele, S.M., Thera, I., Sagara,
1022 I., Sylla, M., Dolo, A., Misidai, N., Simando, S., Msami, H., Juma, O., Gutapaka, N., Paul,
1023 R., Mswata, S., Sasamalo, I., Johaness, K., Sultan, M., Alexander, A., Kimaro, I., Lwanga,
1024 K., Mtungwe, M., Khamis, K., Rugarabam, L., Kalinga, W., Mohammed, M., Kamange,
1025 J., Msangi, J., Mwaijande, B., Mtaka, I., Mhapa, M., Mlaganile, T., Mbaga, T., Yerbanga,
1026 R.S., Samtouma, W., Sienou, A.A., Kabre, Z., Ouedraogo, W.J.M., Yarbanga, G.A.B.,

1027 Zongo, I., Savadogo, H., Sanon, J., Compaore, J., Kere, I., Yoni, F.L., Sanre, T.M.,
1028 Ouattara, S.B., Provstgaard-Morys, S., Woods, D., Snow, R.W., Amek, N., Ngetsa, C.J.,
1029 Ochola-Oyier, L.I., Musyoki, J., Munene, M., Mumba, N., Adetifa, U.J., Muiruri, C.M.,
1030 Mwawaka, J.S., Mwaganyuma, M.H., Ndichu, M.N., Weya, J.O., Njogu, K., Grant, J.,
1031 Webster, J., Lakhkar, A., Ido, N.F.A., Traore, O., Tahita, M.C., Bonko, M. dit A.,
1032 Rouamba, T., Ouedraogo, D.F., Soma, R., Millogo, A., Ouedraogo, E., Sorgho, F.,
1033 Konate, F., Valea, I., 2024. Safety and efficacy of malaria vaccine candidate R21/Matrix-
1034 M in African children: a multicentre, double-blind, randomised, phase 3 trial. The Lancet
1035 403, 533–544. https://doi.org/10.1016/S0140-6736(23)02511-4

1036 Dobin, A., Davis, C.A., Schlesinger, F., Drenkow, J., Zaleski, C., Jha, S., Batut, P., Chaisson,
1037 M., Gingeras, T.R., 2013. STAR: ultrafast universal RNA-seq aligner. Bioinformatics 29,
1038 15–21. https://doi.org/10.1093/bioinformatics/bts635

1039 Douglas, A.D., Williams, A.R., Illingworth, J.J., Kamuyu, G., Biswas, S., Goodman, A.L.,
1040 Wyllie, D.H., Crosnier, C., Miura, K., Wright, G.J., Long, C.A., Osier, F.H., Marsh, K.,
1041 Turner, A. V., Hill, A.V.S., Draper, S.J., 2011. The blood-stage malaria antigen PfRH5 is
1042 susceptible to vaccine-inducible cross-strain neutralizing antibody. Nat Commun 2, 601.
1043 https://doi.org/10.1038/ncomms1615

1044 Duraisingh, M.T., Maier, A.G., Triglia, T., Cowman, A.F., 2003. Erythrocyte-binding antigen
1045 175 mediates invasion in Plasmodium falciparum utilizing sialic acid-dependent and -
1046 independent pathways. Proc Natl Acad Sci U S A 100, 4796–4801.
1047 https://doi.org/10.1073/pnas.0730883100

1048 Eisenhaber, B., Bork, P., Eisenhaber, F., 1999. Prediction of potential GPI-modification sites
1049 in proprotein sequences. J Mol Biol 292, 741–58. https://doi.org/10.1006/jmbi.1999.3069

1050 Escalante, A.A., Cepeda, A.S., Pacheco, M.A., 2022. Why Plasmodium vivax and Plasmodium
1051 falciparum are so different? A tale of two clades and their species diversities. Malar J 21,
1052 139. https://doi.org/10.1186/s12936-022-04130-9

1053 Feng, G., Boyle, M.J., Cross, N., Chan, J.-A., Reiling, L., Osier, F., Stanisic, D.I., Mueller, I.,
1054 Anders, R.F., McCarthy, J.S., Richards, J.S., Beeson, J.G., 2018. Human Immunization
1055 With a Polymorphic Malaria Vaccine Candidate Induced Antibodies to Conserved
1056 Epitopes That Promote Functional Antibodies to Multiple Parasite Strains. J Infect Dis
1057 218, 35–43. https://doi.org/10.1093/infdis/jiy170

1058 Ferreira, E. d'Avila, Alexandre, M.A., Salinas, J.L., de Siqueira, A.M., Benzecry, S.G., de
1059 Lacerda, M.V.G., Monteiro, W.M., 2015. Association between anthropometry-based
1060 nutritional status and malaria: a systematic review of observational studies. Malaria J 14,
1061 346. https://doi.org/10.1186/s12936-015-0870-5

1062 Fowkes, F.J.I., Richards, J.S., Simpson, J.A., Beeson, J.G., 2010. The Relationship between
1063 Anti-merozoite Antibodies and Incidence of Plasmodium falciparum Malaria: A
1064 Systematic Review and Meta-analysis. PLoS Med 7, e1000218.
1065 https://doi.org/10.1371/journal.pmed.1000218

1066 Genton, B., Al-Yaman, F., Betuela, I., Anders, R.F., Saul, A., Baea, K., Mellombo, M.,
1067 Taraika, J., Brown, G. V., Pye, D., Irving, D.O., Felger, I., Beck, H.-P.P., Smith, T.A.,
1068 Alpers, M.P., 2003. Safety and immunogenicity of a three-component blood-stage malaria
1069 vaccine (MSP1, MSP2, RESA) against Plasmodium falciparum in Papua New Guinean
1070 children. Vaccine 22, 30–41. https://doi.org/https://doi.org/10.1016/S0264-
1071 410X(03)00536-X

1072 Genton, B., Betuela, I., Felger, I., Al-Yaman, F., Anders, R.F., Saul, A., Rare, L., Baisor, M.,
1073 Lorry, K., Brown, G. V, Pye, D., Irving, D.O., Smith, T.A., Beck, H.-P., Alpers, M.P.,
1074 2002. A Recombinant Blood-Stage Malaria Vaccine Reduces Plasmodium falciparum
1075 Density and Exerts Selective Pressure on Parasite Populations in a Phase 1-2b Trial in
1076 Papua New Guinea. J Infect Dis 185, 820–827.

1077 Gilson, P.R., Nebl, T., Vukcevic, D., Moritz, R.L., Sargeant, T., Speed, T.P., Schofield, L.,
1078 Crabb, B.S., 2006. Identification and Stoichiometry of Glycosylphosphatidylinositol-
1079 anchored Membrane Proteins of the Human Malaria Parasite *Plasmodium falciparum*.
1080 Molecular & Cellular Proteomics 5, 1286–1299. https://doi.org/10.1074/mcp.M600035-
1081 MCP200

1082 Griffiths, K., Dolezal, O., Cao, B., Nilsson, S.K., See, H.B., Pfleger, K.D.G., Roche, M., Gorry,
1083 P.R., Pow, A., Viduka, K., Lim, K., Lu, B.G.C., Chang, D.H.C., Murray-Rust, T.,
1084 Kvansakul, M., Perugini, M.A., Dogovski, C., Doerflinger, M., Zhang, Y., Parisi, K.,
1085 Casey, J.L., Nuttall, S.D., Foley, M., 2016a. i-bodies, Human Single Domain Antibodies
1086 That Antagonize Chemokine Receptor CXCR4. J Biol Chem 291, 12641–12657.
1087 https://doi.org/10.1074/jbc.M116.721050

1088 Griffiths, K., Habiel, D.M., Jaffar, J., Binder, U., Darby, W.G., Hosking, C.G., Skerra, A.,
1089 Westall, G.P., Hogaboam, C.M., Foley, M., 2018. Anti-fibrotic Effects of CXCR4-

1090 Targeting i-body AD-114 in Preclinical Models of Pulmonary Fibrosis. Sci Rep 8, 3212.
1091 https://doi.org/10.1038/s41598-018-20811-5

1092 Jumper, J., Evans, R., Pritzel, A., Green, T., Figurnov, M., Ronneberger, O., Tunyasuvunakool,
1093 K., Bates, R., Žídek, A., Potapenko, A., Bridgland, A., Meyer, C., Kohl, S.A.A., Ballard,
1094 A.J., Cowie, A., Romera-Paredes, B., Nikolov, S., Jain, R., Adler, J., Back, T., Petersen,
1095 S., Reiman, D., Clancy, E., Zielinski, M., Steinegger, M., Pacholska, M., Berghammer,
1096 T., Bodenstein, S., Silver, D., Vinyals, O., Senior, A.W., Kavukcuoglu, K., Kohli, P.,
1097 Hassabis, D., 2021. Highly accurate protein structure prediction with AlphaFold. Nature
1098 596, 583–589. https://doi.org/10.1038/s41586-021-03819-2

1099 Kals, E., Kals, M., Lees, R.A., Introini, V., Kemp, A., Silvester, E., Collins, C.R., Umrekar,
1100 T., Kotar, J., Cicuta, P., Rayner, J.C., 2024. Application of optical tweezer technology
1101 reveals that PfEBA and PfRH ligands, not PfMSP1, play a central role in Plasmodium
1102 falciparum merozoite-erythrocyte attachment. PLoS Pathog 20, e1012041.
1103 https://doi.org/10.1371/journal.ppat.1012041

1104 Kocken, C.H., van der Wel, A.M., Dubbeld, M.A., Narum, D.L., van de Rijke, F.M., van
1105 Gemert, G.J., van der Linde, X., Bannister, L.H., Janse, C., Waters, A.P., Thomas, A.W.,
1106 1998. Precise timing of expression of a Plasmodium falciparum-derived transgene
1107 in Plasmodium berghei is a critical determinant of subsequent subcellular localization. J
1108 Biol Chem 273, 15119–15124. https://doi.org/10.1074/jbc.273.24.15119

1109 Lamarque, M., Besteiro, S., Papoin, J., Roques, M., Vulliez-Le Normand, B., Morlon-Guyot,
1110 J., Dubremetz, J.-F., Fauquenoy, S., Tomavo, S., Faber, B.W., Kocken, C.H., Thomas,
1111 A.W., Boulanger, M.J., Bentley, G.A., Lebrun, M., 2011. The RON2-AMA1 Interaction
1112 is a Critical Step in Moving Junction-Dependent Invasion by Apicomplexan Parasites.
1113 PLoS Pathog 7, e1001276.

1114 Li, X., Chen, H., Oo, T.H., Daly, T.M., Bergman, L.W., Liu, S.-C., Chishti, A.H., Oh, S.S.,
1115 2004. A co-ligand complex anchors Plasmodium falciparum merozoites to the
1116 erythrocyte invasion receptor band 3. J Biol Chem 279, 5765–5771.
1117 https://doi.org/10.1074/jbc.M308716200

1118 Li, Y., Yang, L., Yang, L.-Q., 2024. Effects of intrinsically disordered regions in gp120
1119 underlying HIV neutralization phenotypes. Biochem Biophys Res Commun 709, 149830.
1120 https://doi.org/10.1016/j.bbrc.2024.149830

1121 Liao, Y., Smyth, G.K., Shi, W., 2014. featureCounts: an efficient general purpose program for
1122 assigning sequence reads to genomic features. Bioinformatics 30, 923–930.
1123 https://doi.org/10.1093/bioinformatics/btt656

1124 Liffner, B., Frölich, S., Heinemann, G.K., Liu, B., Ralph, S.A., Dixon, M.W.A., Gilberger,
1125 T.W., Wilson, D.W., 2020. PfCERLI1 is a conserved rhoptry associated protein essential
1126 for Plasmodium falciparum merozoite invasion of erythrocytes. Nat Commun 11.
1127 https://doi.org/10.1038/s41467-020-15127-w

1128 Livak, K.J., Schmittgen, T.D., 2001. Analysis of Relative Gene Expression Data Using Real-
1129 Time Quantitative PCR and the 2−ΔΔCT Method. Methods 25, 402–408.
1130 https://doi.org/https://doi.org/10.1006/meth.2001.1262

1131 Love, M.I., Huber, W., Anders, S., 2014. Moderated estimation of fold change and dispersion
1132 for RNA-seq data with DESeq2. Genome Biol 15, 550. https://doi.org/10.1186/s13059-
1133 014-0550-8

1134 Lu, C., Zheng, X., Zhang, W., Zhao, H., MacRaild, C.A., Norton, R.S., Zhuang, Y., Wang, J.,
1135 Zhang, X., 2019. Interaction of merozoite surface protein 2 with lipid membranes. FEBS
1136 Lett 593, 288–295. https://doi.org/10.1002/1873-3468.13320

1137 MacRaild, C.A., Pedersen, M.Ø., Anders, R.F., Norton, R.S., 2012. Lipid interactions of the
1138 malaria antigen merozoite surface protein 2. Biochim Biophys Acta 1818, 2572–8.
1139 https://doi.org/10.1016/j.bbamem.2012.06.015

1140 MacRaild, C.A., Zachrdla, M., Andrew, D., Krishnarjuna, B., Nováček, J., Žídek, L., Sklenář,
1141 V., Richards, J.S., Beeson, J.G., Anders, R.F., Norton, R.S., 2015. Conformational
1142 dynamics and antigenicity in the disordered malaria antigen merozoite surface protein 2.
1143 PLoS One 10, e0119899. https://doi.org/10.1371/journal.pone.0119899

1144 McCarthy, J.S., Marjason, J., Elliott, S., Fahey, P., Bang, G., Malkin, E., Tierney, E., Aked-
1145 Hurditch, H., Adda, C., Cross, N., Richards, J.S., Fowkes, F.J.I., Boyle, M.J., Long, C.,
1146 Druilhe, P., Beeson, J.G., Anders, R.F., 2011. A phase 1 trial of MSP2-C1, a blood-stage
1147 malaria vaccine containing 2 isoforms of MSP2 formulated with montanide® ISA 720.
1148 PLoS One 6. https://doi.org/10.1371/journal.pone.0024413

1149 Ocampo, M., Urquiza, M., Guzmán, F., Rodriguez, L.E., Suarez, J., Curtidor, H., Rosas, J.,
1150 Diaz, M., Patarroyo, M.E., 2003. Two MSA 2 peptides that bind to human red blood cells

1151 are relevant to Plasmodium falciparum merozoite invasion. The Journal of Peptide
1152 Research 55, 216–223. https://doi.org/10.1034/j.1399-3011.2000.00174.x

1153 Orlandi, P.A., Klotz, F.W., Haynes, J.D., 1992. A malaria invasion receptor, the 175-kilodalton
1154 erythrocyte binding antigen of Plasmodium falciparum recognizes the terminal Neu5Ac
1155 (alpha 2-3) Gal-sequences of glycophorin A. J Cell Biol 116, 901–909.

1156 Osier, F.H., Feng, G., Boyle, M.J., Langer, C., Zhou, J., Richards, J.S., McCallum, F.J.,
1157 Reiling, L., Jaworowski, A., Anders, R.F., Marsh, K., Beeson, J.G., 2014. Opsonic
1158 phagocytosis of Plasmodium falciparum merozoites: mechanism in human immunity and
1159 a correlate of protection against malaria. BMC Med 12, 108.
1160 https://doi.org/10.1186/1741-7015-12-108

1161 Osier, F.H.A., Murungi, L.M., Fegan, G., Tuju, J., Tetteh, K.K., Bull, P.C., Conway, D.J.,
1162 Marsh, K., 2010. Allele-specific antibodies to Plasmodium falciparum merozoite surface
1163 protein-2 and protection against clinical malaria. Parasite Immunol 32, 193–201.
1164 https://doi.org/10.1111/j.1365-3024.2009.01178.x

1165 Peng, D., Tarleton, R., 2015. EuPaGDT: a web tool tailored to design CRISPR guide RNAs
1166 for eukaryotic pathogens. Microb Genom 1. https://doi.org/10.1099/mgen.0.000033

1167 Persson, K.E.M., Fowkes, F.J.I., McCallum, F.J., Gicheru, N., Reiling, L., Richards, J.S.,
1168 Wilson, D.W., Lopaticki, S., Cowman, A.F., Marsh, K., Beeson, J.G., 2013. Erythrocyte-
1169 Binding Antigens of Plasmodium falciparum Are Targets of Human Inhibitory Antibodies
1170 and Function To Evade Naturally Acquired Immunity. The Journal of Immunology 191,
1171 785–794. https://doi.org/10.4049/jimmunol.1300444

1172 Persson, K.E.M., McCallum, F.J., Reiling, L., Lister, N.A., Stubbs, J., Cowman, A.F., Marsh,
1173 K., Beeson, J.G., 2008. Variation in use of erythrocyte invasion pathways by Plasmodium
1174 falciparum mediates evasion of human inhibitory antibodies. J Clin Invest 118, 342–351.
1175 https://doi.org/10.1172/JCI32138

1176 Reiling, L., Boyle, M.J., White, M.T., Wilson, D.W., Feng, G., Weaver, R., Opi, D.H., Persson,
1177 K.E.M., Richards, J.S., Siba, P.M., Fowkes, F.J.I., Takashima, E., Tsuboi, T., Mueller, I.,
1178 Beeson, J.G., 2019. Targets of complement-fixing antibodies in protective immunity
1179 against malaria in children. Nat Commun 10, 610. https://doi.org/10.1038/s41467-019-
1180 08528-z

1181 Ressurreição, M., Thomas, J.A., Nofal, S.D., Flueck, C., Moon, R.W., Baker, D.A., van Ooij,
1182 C., 2020. Use of a highly specific kinase inhibitor for rapid, simple and precise
1183 synchronization of Plasmodium falciparum and Plasmodium knowlesi asexual blood-
1184 stage parasites. PLoS One 15, e0235798. https://doi.org/10.1371/journal.pone.0235798

1185 Richards, J.S., Arumugam, T.U., Reiling, L., Healer, J., Hodder, A.N., Fowkes, F.J.I., Cross,
1186 N., Langer, C., Takeo, S., Uboldi, A.D., Thompson, J.K., Gilson, P.R., Coppel, R.L., Siba,
1187 P.M., King, C.L., Torii, M., Chitnis, C.E., Narum, D.L., Mueller, I., Crabb, B.S.,
1188 Cowman, A.F., Tsuboi, T., Beeson, J.G., 2013. Identification and Prioritization of
1189 Merozoite Antigens as Targets of Protective Human Immunity to Plasmodium falciparum
1190 Malaria for Vaccine and Biomarker Development. The Journal of Immunology 191, 795
1191 LP – 809.

1192 RTSS Clinical Trials Partnership, 2015. Efficacy and safety of RTS,S/AS01 malaria vaccine
1193 with or without a booster dose in infants and children in Africa: final results of a phase 3,
1194 individually randomised, controlled trial. Lancet 386, 31–45.
1195 https://doi.org/http://dx.doi.org/10.1016/S0140-6736(15)60721-8

1196 Sagara, I., Dicko, A., Ellis, R.D., Fay, M.P., Diawara, S.I., Assadou, M.H., Sissoko, M.S.,
1197 Kone, M., Diallo, A.I., Saye, R., Guindo, M.A., Kante, O., Niambele, M.B., Miura, K.,
1198 Mullen, G.E.D., Pierce, M., Martin, L.B., Dolo, A., Diallo, D.A., Doumbo, O.K., Miller,
1199 L.H., Saul, A., 2009. A randomized controlled phase 2 trial of the blood stage AMA1-
1200 C1/Alhydrogel malaria vaccine in children in Mali. Vaccine 27, 3090–3098.
1201 https://doi.org/10.1016/j.vaccine.2009.03.014

1202 Salanti, A., Staalsoe, T., Lavstsen, T., Jensen, A.T.R., Sowa, M.P.K., Arnot, D.E., Hviid, L.,
1203 Theander, T.G., 2003. Selective upregulation of a single distinctly structured var gene in
1204 chondroitin sulphate A-adhering Plasmodium falciparum involved in pregnancy-
1205 associated malaria. Mol Microbiol 49, 179–191. https://doi.org/10.1046/j.1365-
1206 2958.2003.03570.x

1207 Sanders, P.R., Kats, L.M., Drew, D.R., O'Donnell, R.A., O'Neill, M., Maier, A.G., Coppel,
1208 R.L., Crabb, B.S., 2006. A Set of Glycosylphosphatidyl Inositol-Anchored Membrane
1209 Proteins of Plasmodium falciparum Is Refractory to Genetic Deletion. Infect Immun 74,
1210 4330–4338. https://doi.org/10.1128/IAI.00054-06

1211 Scally, S.W., Triglia, T., Evelyn, C., Seager, B.A., Pasternak, M., Lim, P.S., Healer, J.,
1212 Geoghegan, N.D., Adair, A., Tham, W.-H., Dagley, L.F., Rogers, K.L., Cowman, A.F.,

1213 2022. PCRCR complex is essential for invasion of human erythrocytes by Plasmodium
1214 falciparum. Nat Microbiol 7, 2039–2053. https://doi.org/10.1038/s41564-022-01261-2

1215 Sheehy, S.H., Duncan, C.J.A., Elias, S.C., Choudhary, P., Biswas, S., Halstead, F.D., Collins,
1216 K.A., Edwards, N.J., Douglas, A.D., Anagnostou, N.A., Ewer, K.J., Havelock, T.,
1217 Mahungu, T., Bliss, C.M., Miura, K., Poulton, I.D., Lillie, P.J., Antrobus, R.D., Berrie,
1218 E., Moyle, S., Gantlett, K., Colloca, S., Cortese, R., Long, C.A., Sinden, R.E., Gilbert,
1219 S.C., Lawrie, A.M., Doherty, T., Faust, S.N., Nicosia, A., Hill, A.V.S., Draper, S.J., 2012.
1220 ChAd63-MVA-vectored blood-stage malaria vaccines targeting MSP1 and AMA1:
1221 assessment of efficacy against mosquito bite challenge in humans. Mol Ther 20, 2355–
1222 2368. https://doi.org/10.1038/mt.2012.223

1223 Smythe, J.A., Coppel, R.L., Day, K.P., Martin, R.K., Oduola, A.M., Kemp, D.J., Anders, R.F.,
1224 1991. Structural diversity in the Plasmodium falciparum merozoite surface antigen 2.
1225 Proceedings of the National Academy of Sciences 88, 1751 LP – 1755.
1226 https://doi.org/10.1073/pnas.88.5.1751

1227 Srinivasan, P., Beatty, W.L., Diouf, A., Herrera, R., Ambroggio, X., Moch, J.K., Tyler, J.S.,
1228 Narum, D.L., Pierce, S.K., Boothroyd, J.C., Haynes, J.D., Miller, L.H., 2011. Binding of
1229 Plasmodium merozoite proteins RON2 and AMA1 triggers commitment to invasion.
1230 Proceedings of the National Academy of Sciences 108, 13275–13280.
1231 https://doi.org/10.1073/pnas.1110303108

1232 Stanisic, D.I., Richards, J.S., McCallum, F.J., Michon, P., King, C.L., Schoepflin, S., Gilson,
1233 P.R., Murphy, V.J., Anders, R.F., Mueller, I., Beeson, J.G., 2009. Immunoglobulin G
1234 Subclass-Specific Responses against Plasmodium falciparum Merozoite Antigens Are
1235 Associated with Control of Parasitemia and Protection from Symptomatic Illness. Infect
1236 Immun 77, 1165–1174. https://doi.org/10.1128/IAI.01129-08

1237 Stejskal, L., Kalemera, M.D., Lewis, C.B., Palor, M., Walker, L., Daviter, T., Lees, W.D.,
1238 Moss, D.S., Kremyda-Vlachou, M., Kozlakidis, Z., Gallo, G., Bailey, D., Rosenberg, W.,
1239 Illingworth, C.J.R., Shepherd, A.J., Grove, J., 2022. An entropic safety catch controls
1240 hepatitis C virus entry and antibody resistance. Elife 11.
1241 https://doi.org/10.7554/eLife.71854

1242 Tamura, K., Stecher, G., Kumar, S., 2021. MEGA11: Molecular Evolutionary Genetics
1243 Analysis Version 11. Mol Biol Evol 38, 3022–3027.
1244 https://doi.org/10.1093/molbev/msab120

1245 Taylor, H.M., McRobert, L., Grainger, M., Sicard, A., Dluzewski, A.R., Hopp, C.S., Holder,
1246 A.A., Baker, D.A., 2010. The malaria parasite cyclic GMP-dependent protein kinase plays
1247 a central role in blood-stage schizogony. Eukaryot Cell 9, 37–45.
1248 https://doi.org/10.1128/EC.00186-09

1249 Thera, M.A., Doumbo, O.K., Coulibaly, D., Laurens, M.B., Ouattara, A., Kone, A.K., Guindo,
1250 A.B., Traore, K., Traore, I., Kouriba, B., Diallo, D.A., Diarra, I., Daou, M., Dolo, A.,
1251 Tolo, Y., Sissoko, M.S., Niangaly, A., Sissoko, M., Takala-Harrison, S., Lyke, K.E., Wu,
1252 Y., Blackwelder, W.C., Godeaux, O., Vekemans, J., Dubois, M.-C., Ballou, W.R., Cohen,
1253 J., Thompson, D., Dube, T., Soisson, L., Diggs, C.L., House, B., Lanar, D.E., Dutta, S.,
1254 Heppner, D.G., Plowe, C. V., 2011. A Field Trial to Assess a Blood-Stage Malaria
1255 Vaccine. New England Journal of Medicine 365, 1004–1013.
1256 https://doi.org/10.1056/NEJMoa1008115

1257 Weiss, G.E., Gilson, P.R., Taechalertpaisarn, T., Tham, W.-H.H., de Jong, N.W.M.M., Harvey,
1258 K.L., Fowkes, F.J.I.I., Barlow, P.N., Rayner, J.C., Wright, G.J., Cowman, A.F., Crabb,
1259 B.S., 2015. Revealing the Sequence and Resulting Cellular Morphology of Receptor-
1260 Ligand Interactions during Plasmodium falciparum Invasion of Erythrocytes. PLoS
1261 Pathog 11, 284–295. https://doi.org/10.1371/journal.ppat.1004670

1262 Wickham, H., 2016. ggplot2: Elegant Graphics for Data Analysis. Springer-Verlag New York.

1263 Wilson, D.W., Goodman, C.D., Sleebs, B.E., Weiss, G.E., de Jong, N.W.M., Angrisano, F.,
1264 Langer, C., Baum, J., Crabb, B.S., Gilson, P.R., McFadden, G.I., Beeson, J.G., 2015.
1265 Macrolides rapidly inhibit red blood cell invasion by the human malaria parasite,
1266 Plasmodium falciparum. BMC Biol 13, 52. https://doi.org/10.1186/s12915-015-0162-0

1267 World Health Organization, 2024. World malaria report 2024: addressing inequity in the global
1268 malaria response. World Health Organization, Geneva.

1269 Yang, X., Adda, C.G., MacRaild, C.A., Low, A., Zhang, X., Zeng, W., Jackson, D.C., Anders,
1270 R.F., Norton, R.S., 2010. Identification of key residues involved in fibril formation by the
1271 conserved N-terminal region of Plasmodium falciparum merozoite surface protein 2
1272 (MSP2). Biochimie 92, 1287–95. https://doi.org/10.1016/j.biochi.2010.06.001

1273 Zerebinski, J., Margerie, L., Han, N.S., Moll, M., Ritvos, M., Jahnmatz, P., Ahlborg, N.,
1274 Ngasala, B., Rooth, I., Sjöberg, R., Sundling, C., Yman, V., Färnert, A., Plaza, D.F., 2024.
1275 Naturally acquired IgG responses to Plasmodium falciparum do not target the conserved

termini of the malaria vaccine candidate Merozoite Surface Protein 2. Front Immunol 15, 1501700. https://doi.org/10.3389/fimmu.2024.1501700

Zhang, X., Adda, C.G., Low, A., Zhang, J., Zhang, W., Sun, H., Tu, X., Anders, R.F., Norton, R.S., 2012. Role of the helical structure of the N-terminal region of plasmodium falciparum merozoite surface protein 2 in fibril formation and membrane interaction. Biochemistry 51, 1380–1387. https://doi.org/10.1021/bi201880s

Zhang, X., Perugini, M.A., Yao, S., Adda, C.G., Murphy, V.J., Low, A., Anders, R.F., Norton, R.S., 2008. Solution conformation, backbone dynamics and lipid interactions of the intrinsically unstructured malaria surface protein MSP2. J Mol Biol 379, 105–21. https://doi.org/10.1016/j.jmb.2008.03.039